



UvA-DARE (Digital Academic Repository)

Bending benzenes and twisting light

Kovida, K.

Publication date
2026

[Link to publication](#)

Citation for published version (APA):

Kovida, K. (2026). *Bending benzenes and twisting light*. [Thesis, fully internal, Universiteit van Amsterdam].

General rights

It is not permitted to download or to forward/distribute the text or part of it without the consent of the author(s) and/or copyright holder(s), other than for strictly personal, individual use, unless the work is under an open content license (like Creative Commons).

Disclaimer/Complaints regulations

If you believe that digital publication of certain material infringes any of your rights or (privacy) interests, please let the Library know, stating your reasons. In case of a legitimate complaint, the Library will make the material inaccessible and/or remove it from the website. Please Ask the Library: <https://uba.uva.nl/en/contact>, or a letter to: Library of the University of Amsterdam, Secretariat, P.O. Box 19185, 1000 GD Amsterdam, The Netherlands. You will be contacted as soon as possible.

2

[2.2]paracyclophane-based Chiral Carbon Nanohoops

This chapter is to be published: Kovida K.; Šolomek T. [2.2]PCP-based Chiral Carbon Nanohoops.

Abstract

[2.2]paracyclophane (PCP) represents a unique scaffold distinguished by its rigid, co-facial benzene rings and through-space π - π interactions, permitting planar chirality. These features make it a versatile chiral building block for constructing optically active π -conjugated systems. In parallel, cycloparaphenylenes ([n]CPPs) have emerged as model systems for studying curvature-dependent conjugation, strain and photophysical behavior in confined π -systems. The integration of PCP units into CPP frameworks offers an appealing strategy to merge planar chirality with radial π -conjugation within a single conjugated architecture, enabling construction of configurationally stable chiroptical materials.

In this chapter, I present the conceptual design and synthetic realization of PCP-based chiral carbon nano hoops. The approach exploits modular building blocks derived from pseudo-*meta*-disubstituted and tetra-substituted PCP derivatives, allowing precise control over substitution geometry and orientation. Particular emphasis is placed on the synthetic constraints imposed by strain accumulation during aromatization and the resulting configurational and chemical stability. The design rationale guiding the transition from planar to topologically chiral architectures is discussed in the context of competing reports.

2.1 Introduction

Paracyclophane (PCP) represents one of the most distinctive aromatic scaffolds in organic chemistry, first discovered serendipitously by Brown and Farthing in 1949 through vapor-phase pyrolysis of *p*-xylene.¹⁻³ This fascinating molecule consists of two benzene rings bound together by two ethylene bridges creating a highly strained structure with a strain energy of 31 kcal mol⁻¹. The close proximity of the aromatic rings, with distances ranging from 2.78 Å to 3.09 Å, significantly shorter than the expected van der Waals distance of 3.40 Å, forces each benzene ring into a flattened boat conformation and prevents free rotation, making the compound stable up to approximately 200 °C.⁴

The structural constraints imposed by the ethylene bridges create one of the PCP's most important features: **planar chirality**. While unsubstituted PCP belongs to D_{2h} symmetry, introduction of even a single substituent breaks this symmetry, resulting in two planar chiral enantiomers that cannot be interconverted through rotation. The co-facially stacked benzene rings enable unusual transannular π - π electronic interactions via both “through-space” and “through-bond” pathways.^{3,5-7} This electronic communication, combined with the rigid, stable and planar nature have driven its evolution from a chemical curiosity to applications ranging from asymmetric catalysis to advanced optical materials.⁸⁻¹¹

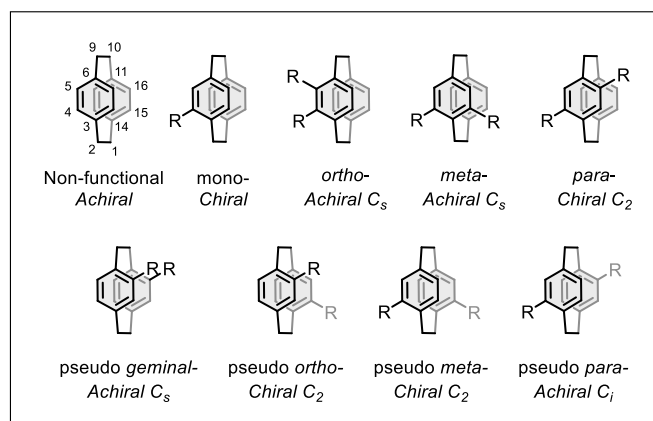


Figure 2.1. Common substitution patterns of mono- and di-substituted [2.2]paracyclophane.

The modular nature of the PCP core allows for selective incorporation of functional groups on either benzene rings, enabling the synthesis of mono- and differently functionalized regioisomers including pseudo-*geminal*, pseudo-*ortho*, pseudo-*meta* and pseudo-*para* disubstituted derivatives (Figure 2.1).¹²⁻¹⁴ The prefix “pseudo” (ps) is used when two substituents are positioned on different

decks of the PCP scaffold. This geometric distinction, while subtle at first glance, plays a decisive role in how PCP derivatives behave electronically, sterically and optically.^{15–17}

The planar chirality and intrinsic fluorescence of PCP have made it particularly valuable for developing chiroptical materials.^{18–21} Pioneering work by Morisaki and Chujo demonstrated the potential of these systems, achieving high dissymmetry factors of $|g_{\text{lum}}| = 1.1 \times 10^{-2}$ with Φ_{FI} of 45% in propeller-shaped macrocycles based on tetrasubstituted-[2.2]PCP (Figure 2.2a).¹⁹ Later, Hasegawa and co-workers introduced para-phenylene fluorophore onto chiral dibrominated PCP cores producing compounds with Φ_{FI} of 0.20–0.64 and $|g_{\text{lum}}| = 1.5–4.2 \times 10^{-3}$ (Figure 2.2b).²² This approach was further extended to oligothiophene systems, demonstrating the broad applicability of PCP cores for incorporating various π -conjugated systems.¹⁸

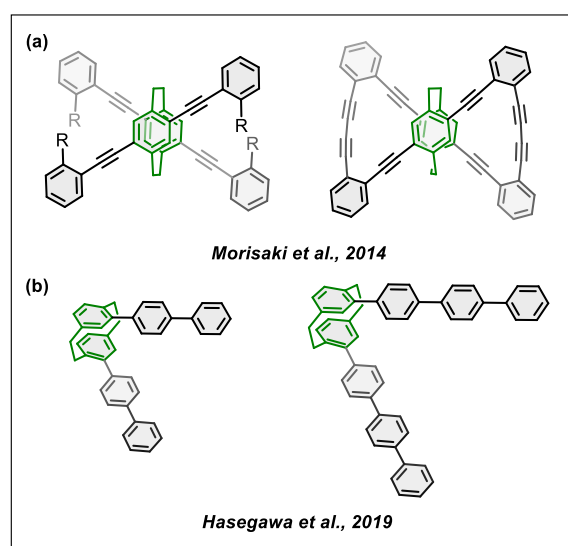


Figure 2.2. Literature work on simple PCP-based systems.^{19,22}

Running parallel to the exploration of PCP, the field of carbon nano hoops has undergone a dramatic expansion over the past two decades. Beyond the “simple” CPPs, interestingly complex architectures including lemniscular i.e., figure-eight carbon macrocycles have been realized for chiroptical applications as discussed in Chapter 1.^{23–30} Given these parallel developments, it is perhaps unsurprising that chemists have sought to merge the distinctive features of PCP and CPPs: PCP offers inherent planar chirality and tunable through-space interactions, while CPPs contribute radial π -conjugation and size-dependent photophysical behavior. Therefore, embedding PCP motifs into CPP frameworks in varying shapes and sizes provides an elegant way to break symmetry, modulate electronic communication and introduce chirality.

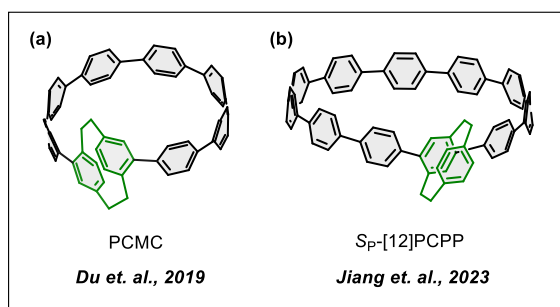


Figure 2.3. Literature systems relevant to this work.^{31,32}

Only a few studies have explored the incorporation of PCP units into CPPs for different applications. Du and co-workers reported the first through-space conjugated macrocycle by integrating pseudo-*para* [2.2]PCP into a [7]CPP framework (Figure 2.3a).³¹ However, its chiroptical properties could not be determined due to rapid racemization of the nano hoop ($\Delta G_{\text{rac}} = 36 \text{ kJ mol}^{-1}$). More recently, in 2023, Jiang and co-workers synthesized S_P-/R_P-[12]PCPP (Figure 2.3b), which can host protonated chiral amines complexed with 18-Crown-6 to form ternary host-guest complexes exhibiting enhanced CD signals.³² Nevertheless, detailed chiroptical properties were not reported for this system either.

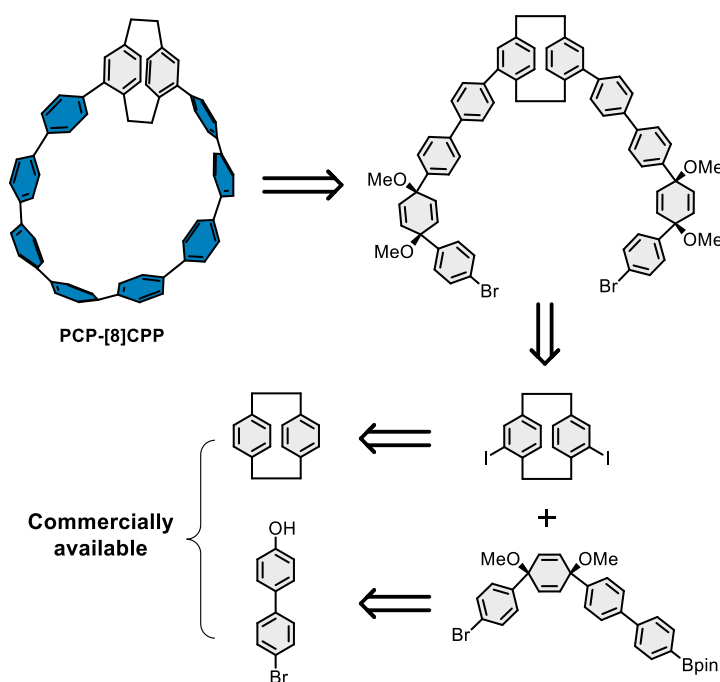
Competitive Studies

In our own investigations, we initially pursued the design of pseudo-*meta* [2.2]PCP-based chiral nano hoops (Scheme 2.1). However, before the completion of our work, two competitive studies were reported. These results will also be discussed in the chapter. Rather than viewing these reports as setbacks, we considered them valuable milestones that helped refine our designs.

This chapter presents the outcome of these efforts, detailing the design and synthesis of [2.2]PCP-based chiral nano hoops with controlled shapes, sizes and geometries. Through systematic tuning of electronic communication between the PCP chiral core and appended chromophores, we aim to provide fundamental insight into how bright CPL emitters can be achieved. To distinguish our approach further, we incorporated an electron-accepting unit, benzothiadiazole (BTD), into tetra-substituted PCP frameworks. This modification not only introduced new pathways towards red-emitting nano hoops but also differentiated our systems from previously reported architectures.

2.2 Results and Discussion

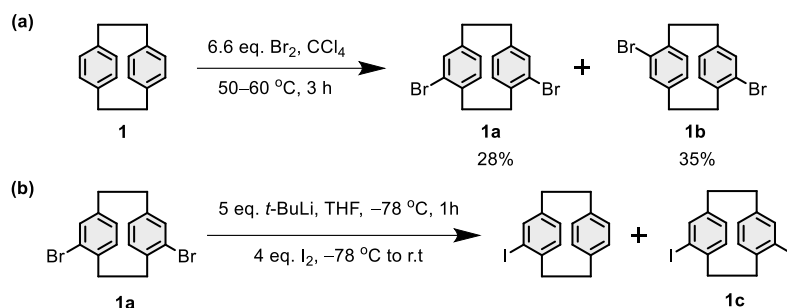
The retrosynthetic analysis of the target molecule is summarized in Scheme 2.1. The design incorporates a planar chiral pseudo-*meta*-disubstituted [2.2]PCP into a [8]CPP framework. This orientation can ensure efficient chirality transfer from PCP to CPP and also afford a configurationally stable system while suppressing racemization to enable the isolation of enantiomers and subsequent chiroptical measurements. A pseudo-*para* connection, by contrast, would require additional substituents at the remaining positions to prevent racemization, a transformation that is synthetically demanding.³³ Accordingly, the synthesis of the target nano hoop was divided into two parts: (i) preparation of the chiral pseudo-*meta*-disubstituted [2.2]PCP fragment, and (ii) construction of the curved CPP segment.



Scheme 2.1. Target molecule retrosynthesis.

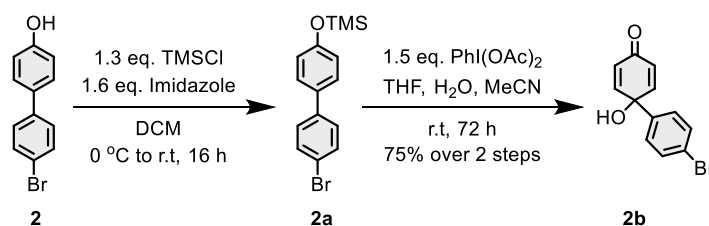
As depicted in Scheme 2.2, bromination of [2.2]PCP provides access to key disubstituted scaffolds. Classical electrophilic bromination with Br₂, sometimes catalyzed by Fe or FeBr₃, typically yields mixtures of mono-, di- and higher brominated derivatives. The isomeric distribution is dictated by the characteristic transannular interactions of the PCP scaffold, often favoring 4,16-substitution (pseudo-*para*) but still producing multiple isomers that require laborious separation.

In our synthesis, commercially available [2.2]PCP **1** was first brominated following procedures from Hopf and co-workers (Scheme 2.2a).¹³ While the literature employs CCl_4 as solvent, we explored less hazardous alternatives (CHCl_3 , CH_2Cl_2). These, however, afforded complex mixtures of regioisomer with low yield of the desired regioisomer. Bromination in CCl_4 finally provided a roughly 1:1 mixture of pseudo-*meta* **1a** and pseudo-*para* **1b** dibromides, from which the pseudo-*meta* dibromide **1a** was isolated in 28% yield after repeated recrystallizations from CH_2Cl_2 .



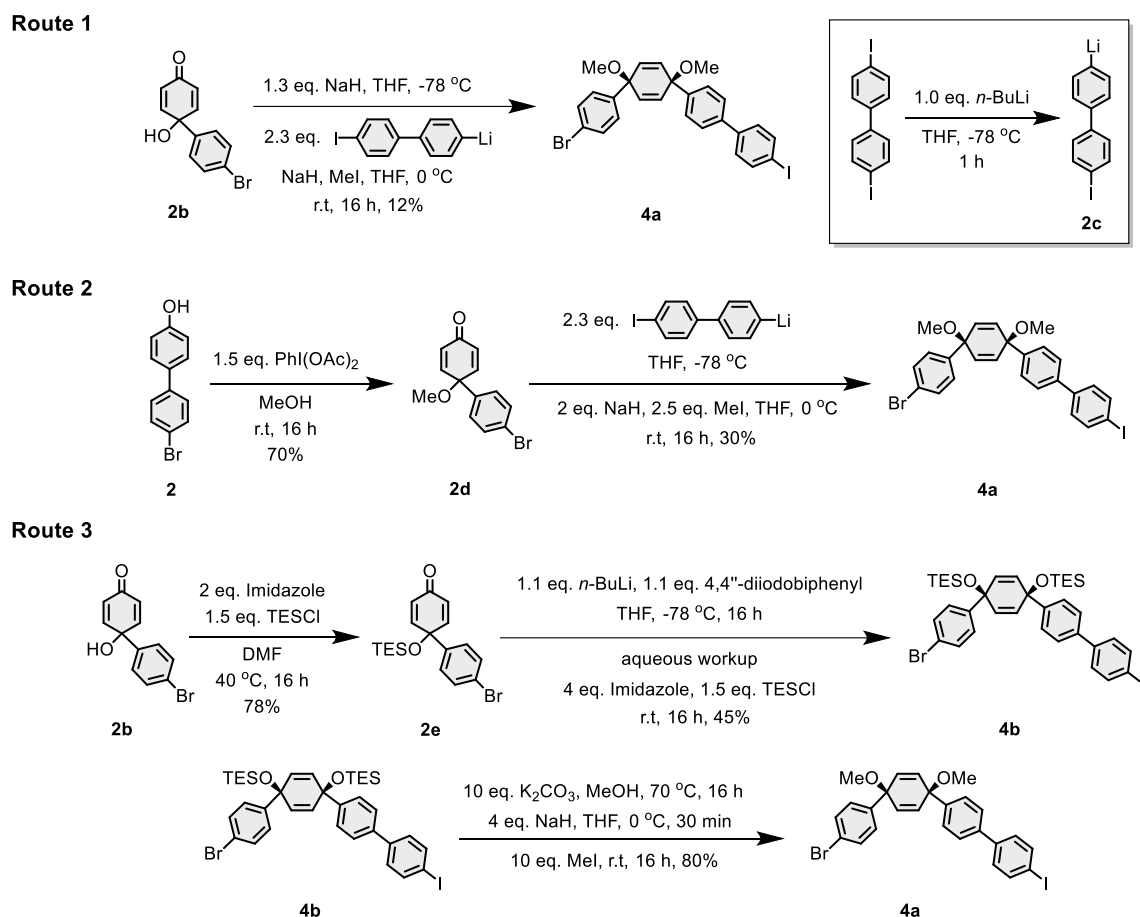
Scheme 2.2. Synthesis of di-substituted [2.2]PCP-based building blocks.^{12,13}

Conversion of pseudo-*meta* dibromide **1a** to the corresponding diiodide **1c** was attempted via lithium-halogen exchange with *t*-BuLi followed by iodination (Scheme 2.2b).¹² However, this approach generated mixtures of mono and diiodides which were difficult to separate. While optimizing these conditions, we moved to the preparation of CPP building blocks as mentioned below.



Scheme 2.3. Synthesis of masked building blocks for cycloparaphenylene synthesis.³⁴

The CPP fragment was assembled using established strategies pioneered by Jasti and co-workers (Scheme 2.3).³⁴ The synthesis commenced with protection of commercially available 4-bromo-1-hydroxy biphenyl **2** using trimethylsilyl chloride and imidazole to yield the silyl protected bromophenol **2a**. Oxidative dearomatization afforded the corresponding ketone **2b** in 75% yield over two steps.



Scheme 2.4. Design strategies towards four-membered masked building blocks.

To afford the four-ring building block **4a**, multiple strategies were employed (Scheme 2.4). According to Route 1, ketone **2b** undergoes deprotonation with sodium hydride at low temperature, followed by nucleophilic addition of the aryllithium **2c**. The route involves an aqueous workup before subsequent methylation at 0 °C using iodomethane affording the dimethyl ether **4a** in 12% yield. Route 2 starts with the protection of phenol **2** to afford **2d** followed by nucleophilic addition of an aryllithium and a second protection sequence. This sequence, although is higher yielding as compared to Route 1, but gives a mixture of *syn*- and *anti*- isomers (~3:1 ratio) requiring a chromatographic separation while Route 1 is stereoselective. Route 3 involves the use of TES protection groups instead of Me groups. Protection of ketone **2b** with TESCl affords **2e** in 78% yield which upon nucleophilic addition and a second protection affords **4b** in 45% yield. This route is overall a high yielding sequence; however, TES groups decompose more easily as compared to Me groups. This can be circumvented by converting it to **4a** via deprotection-protection sequence.³⁵

Competitive Study 1:

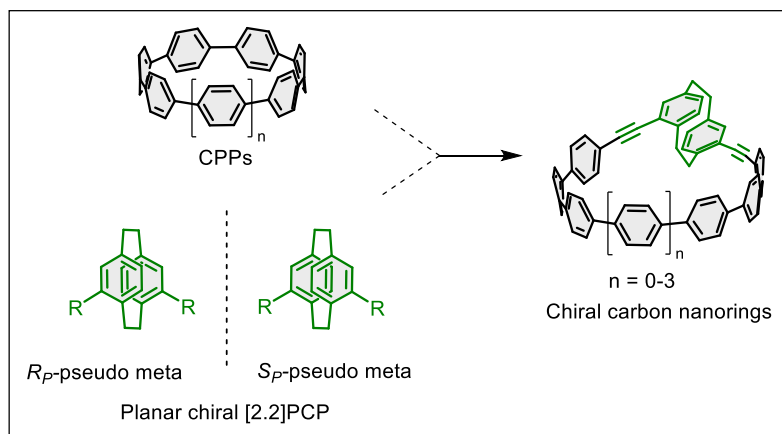


Figure 2.4. Synthetic design based on the integration of CPPs with a planar chiral [2.2]PCP (adapted from Ref³⁶).

At this stage of the synthesis progress, a competitive study on the design and synthesis of [2.2]PCP-based chiral carbon nanohoops was reported by He and co-workers (Figure 2.4).³⁶ The authors synthesized a series of chiral carbon nanohoops (**PCP[6-9]CPPs**) incorporating the planar chiral [2.2]PCP units in a pseudo-*meta* connection, shown to adopt necklace-like conformations. A key difference in the two designs is that their design incorporates acetylenes as linkers between paraphenylenes and the PCP unit. Photophysically, the macrocycles exhibited intense fluorescence with quantum yields reaching up to 82% for largest size, while large blue-shifting fluorescence was observed with increasing ring sizes. Chiroptical properties revealed that $|g_{\text{abs}}|$ values decrease from 3.5×10^{-3} to 2.3×10^{-3} for **PCP-[6~9]CPP** respectively. Same trend was also observed in CPL with $|g_{\text{lum}}|$ values ranging from 2.9×10^{-3} to 1.9×10^{-3} for **PCP-[6~9]CPPs**, typical of small organic molecules ($g_{\text{lum}} = 10^{-5}$ - 10^{-3}). Authors state that the decrease in g values with increasing number of benzene rings is attributed to the fact that chirality transfer from PCP to the rest of the macrocycle becomes less efficient with increase ring size.

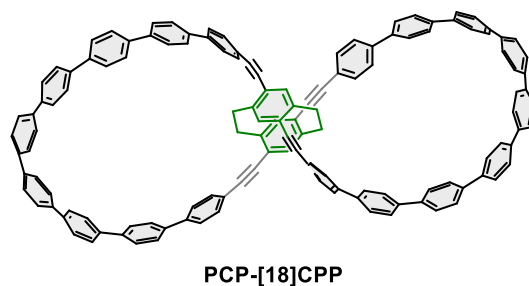
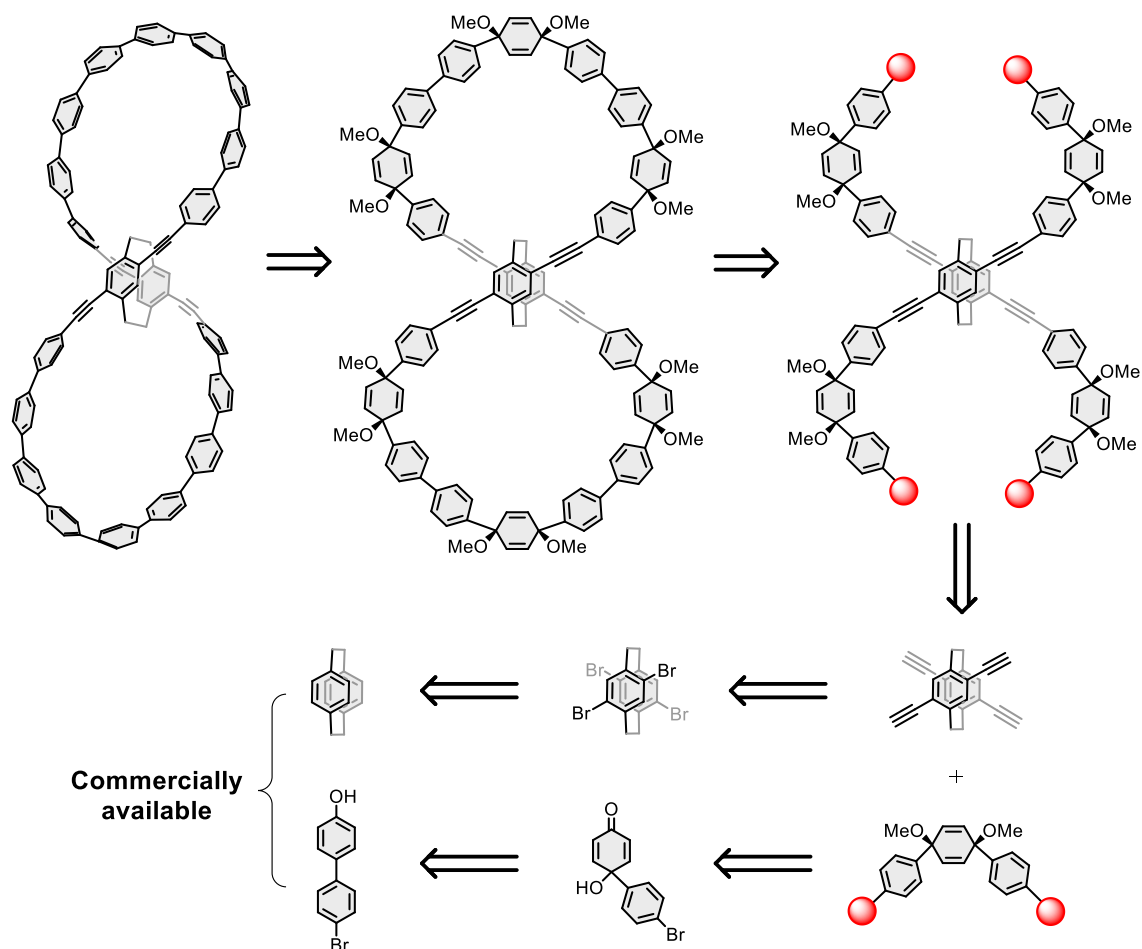
Design and synthesis of [2.2]PCP based chiral carbon double hoop:

Figure 2.5. Structure of target chiral double hoop **PCP-[18]CPP**.

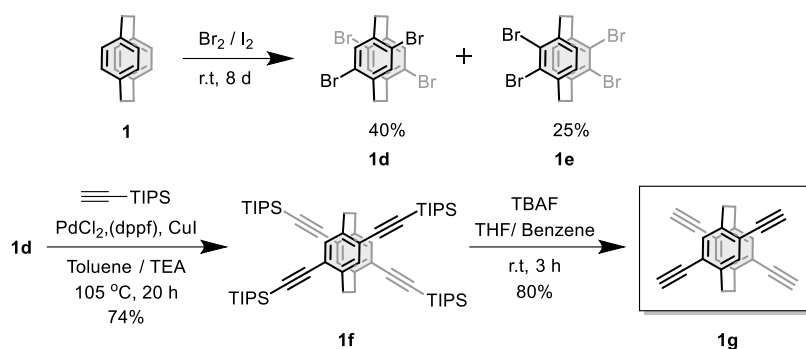
After the unexpected overlap with the competing publication, we refined our design strategy to target a figure-eight nanohoop (Figure 2.5). As discussed in Chapter 1, design of a figure-eight [5]helicene dimer resulted in D_2 point group as the highest symmetry.³⁷ This results in a parallel arrangement of the electric (μ) and magnetic transition dipole moment (m), resulting in high value of $\cos\theta$ and thus higher g_{lum} . This study provided an inspiration for our design to incorporate a chiral 3D building block, namely, tetra-substituted [2.2]PCP into the CPP scaffold to produce a configurationally stable, electronically delocalized system owing to the transannular interactions between the benzene rings of [2.2]PCP thus leading to favorable chiroptical properties.

Retrosynthetic analysis towards target nanohoop: Based on above design strategy, we targeted a large carbon nanohoop consisting of 18 phenylene units, arranged as two loops of nine phenylenes each (Figure 2.5). The corresponding retrosynthesis for this target nanohoop is depicted in Scheme 2.5, outlining the key disconnections and synthetic strategy. The nanohoop can be realized from a strain-free precursor that employs cyclohexadienes as masked benzene rings, which upon aromatization would generate the final strained nanohoop structure. This strategy allows the macrocycle to be constructed under mild conditions in a less strained, flexible form with strain only introduced at the final step. The *pro*-aromatic precursor can be efficiently assembled through cross-coupling reactions between modular aryl-alkyne building blocks, all of which are accessible via well-established synthetic methodologies from commercially available precursors. The synthesis thus enables a controlled synthesis of the figure-eight carbon nanohoop.



Scheme 2.5. Retrosynthesis for target figure-eight double hoop PCP-[18]CPP.

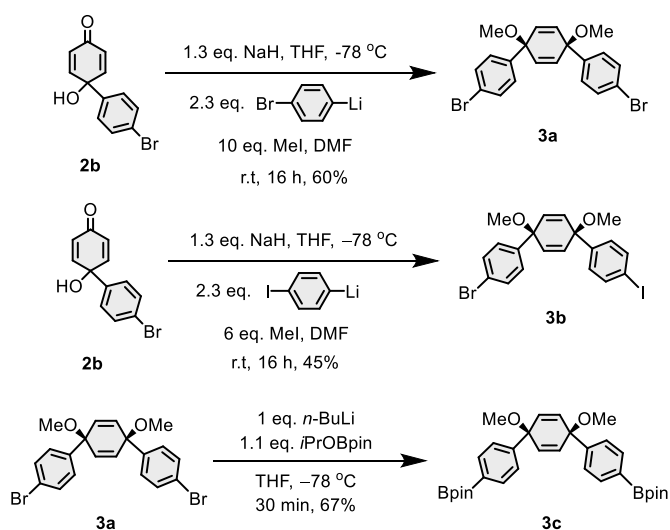
Synthesis of tetra-substituted [2.2]PCP building blocks: First, the commercial [2.2]PCP **1** was brominated to yield a mixture of two regioisomers, tetrabromo[2.2]PCPs **1d** and **1e** (Scheme 2.6).³⁸ The reported procedure achieves separation of two isomers by crystallization from dichloromethane followed by chromatography. However, the minimal difference in retention times renders chromatographic purification inefficient and impractical on large scale. To circumvent this limitation, improved crystallization protocol was developed that eliminated the need for extensive chromatography. Several solvent systems including toluene, chloroform and diethyl ether were systematically evaluated without success. Ultimately, dissolving the isomeric mixture in methyl tert-butyl ether (MTBE) at reflux, followed by gradual cooling to room temperature and slow addition of methanol, afforded well-defined crystals of the desired chiral isomer **1d** in 40% yield.



Scheme 2.6. Synthesis of tetra-substituted [2.2]PCP linkers.

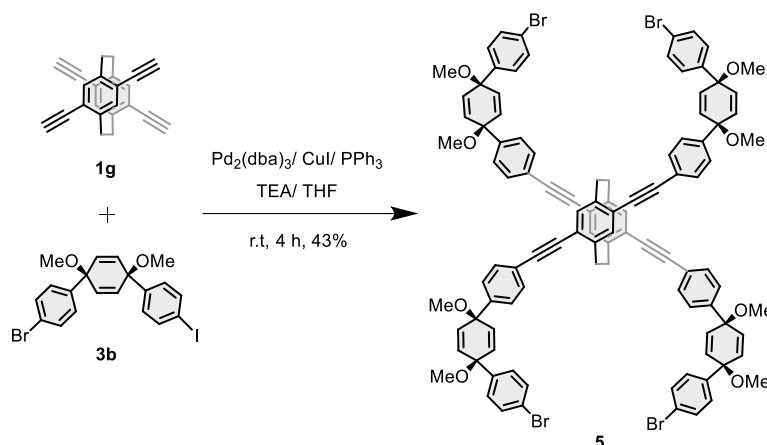
The introduction of acetylene functionalities on the PCP core was achieved via an improved procedure by Krasnova and co-workers.³⁹ Accordingly, Sonogashira cross-coupling reaction of **1d** with triisopropylsilylacetylene (TIPSA) provided the tetra(triisopropylsilylethynyl)[2.2]PCP **1f**, bearing four protected ethynyl groups, in 74% yield. Subsequent deprotection of TIPS groups with tetrabutylammonium fluoride (TBAF) cleanly generated **1g**, which served as a key intermediate for subsequent C–C bond forming reactions to extend the conjugation. Notably, all intermediate compounds from **1d** to the final linker **1g** were efficiently purified by crystallization, thereby ensuring both scalability and high overall yield.

Preparation of CPP building blocks: The CPP components of the target design follow the well-established methodology reported by Jasti and co-workers (Scheme 2.7).^{34,40–42} The previously described ketone **2b** was transformed into the masked three-ring fragments **3a–3b** through a sequence of nucleophilic addition and methylation, in 45–60% yields.

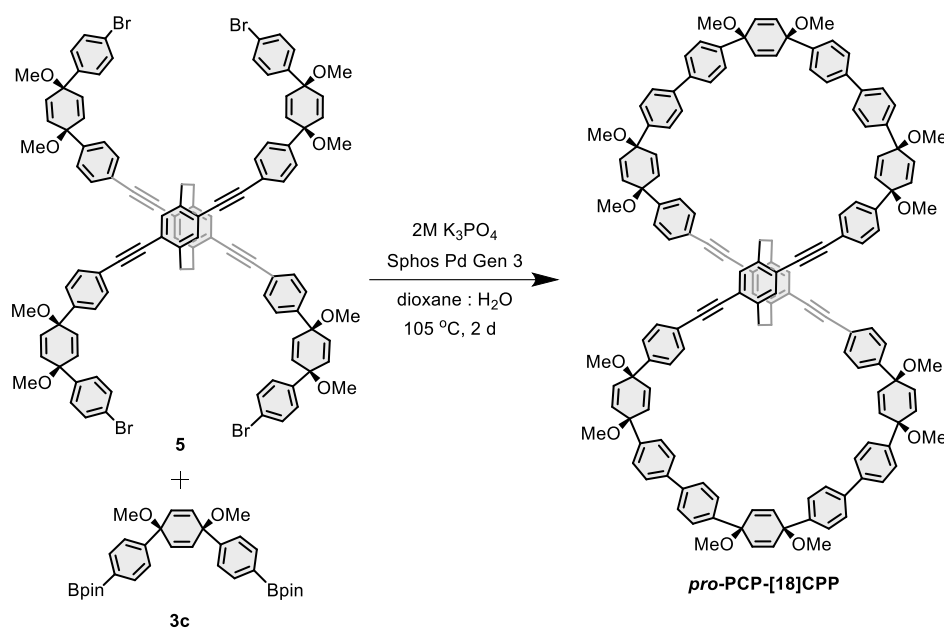


Scheme 2.7. Synthesis of three-ring building blocks.

The tetra-ethynyl PCP linker **1g** was coupled with the three-ring CPP unit **3b** under Sonogashira-Hagihara coupling conditions (Scheme 2.8). The use of Br-I building block **3b** proved optimal as it allowed to perform the cross-coupling reaction at room temperature, providing the desired X-shaped intermediate **5** in 43% yield, after purification by column chromatography followed by gel permeation chromatography by GPC in CHCl_3 (Figure A2.2-A2.4).



Scheme 2.8. Connecting the two linkers to afford X-shaped molecule **5**.



Scheme 2.9. Macrocyclization: for the sake of simplicity, only one isomer is shown.

Macrocyclization and regioisomers: Borylation of the dibromo building block **3a** furnished the corresponding bis(boronate ester) derivative **3c** in 67% yield (Scheme 2.7), which served as a key coupling partner in the macrocyclization step. Macrocyclization of **5** with **3c** was accomplished via

a Suzuki coupling, affording the pro-aromatic macrocyclic precursor, *pro*-PCP-[18]CPP (Scheme 2.9), along with undesired polymeric byproducts. Screenings of the reaction conditions were performed first via varying the concentration of the reaction mixture from 0.3 mM to 37 mM where 10 mM concentration provided optimal results and least amounts of polymeric side products (monitored by GPC). Further temperature screening concluded an increase in the yield of macrocyclization at elevated temperatures (105°C) as compared to 80 °C. Interestingly, a stoichiometric amount of catalyst resulted in improved macrocyclization yields reaching 17% after optimizations. These synthetic challenges and optimizations further proves the difficulty of cross-coupling reactions and low overall yields in the field of carbon nano hoops. The ¹H NMR spectrum of the macrocycle (purified by GPC in chloroform) displayed broad, poorly resolved resonances, suggesting a rapid phenylene rotation at the NMR time scale. Therefore, the formation of the macrocycle was confirmed by high resolution MALDI-MS (Figure A2.5-A2.6).

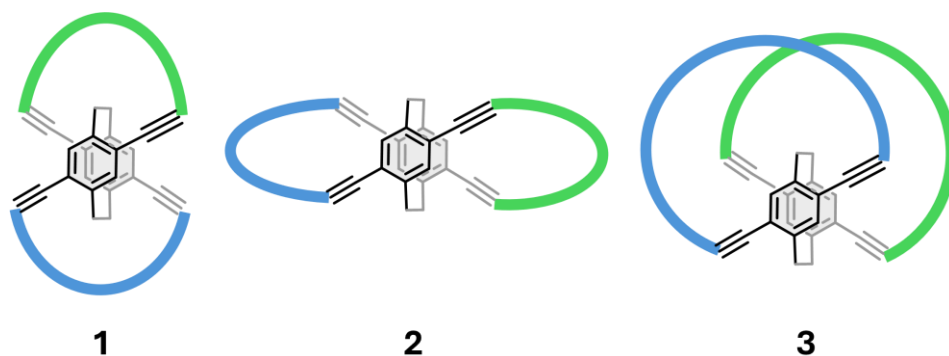
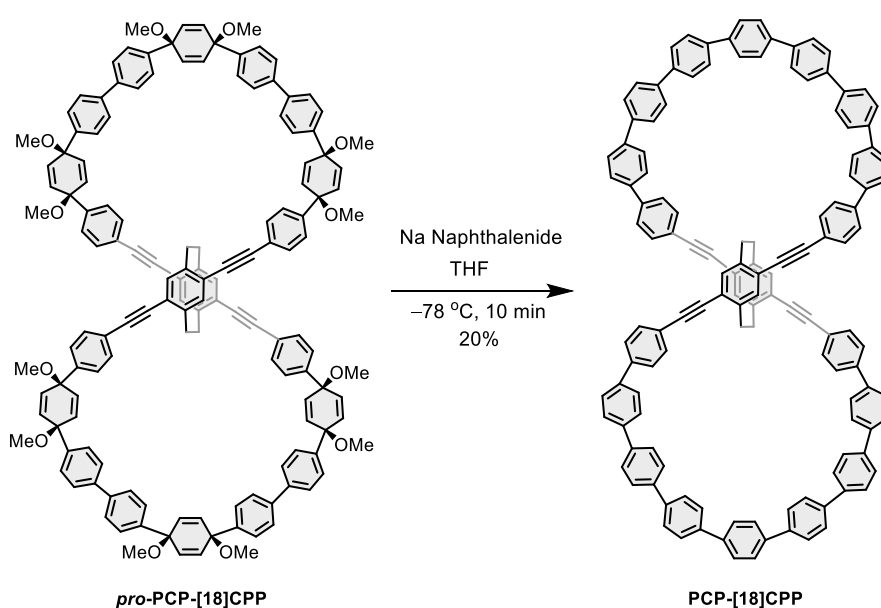


Figure 2.6. Possible regioisomers upon macrocyclization.

It should be noted that the flexible intermediate **5** possesses four rotatable arms, capable of cyclizing in three likely distinct arrangements (Figure 2.6), leading to the formation of three macrocyclic regioisomers. These isomers are expected to be difficult, if not impossible, to separate using standard chromatographic techniques (GPC or silica gel column chromatography). According to our molecular modelling studies, isomer 3 (Figure 2.6) is the most strained of all isomers with lowest probability of formation and we expected one of the two remaining isomers to form. However, figuring out which exact isomer forms has proven to be difficult. The best way to conclude the nature of formed isomer is by crystallization approach, however our attempts towards crystallizations were unsuccessful so far. Given these constraints, the synthesis was advanced to the aromatization stage without further purification of the macrocycle.

Reductive aromatization towards fully conjugated nano hoop: The final reductive aromatization step, aimed at converting the cyclohexadiene moieties into fully aromatic benzene rings, represented the most technically demanding stage of the synthesis (Scheme 2.10). Reductive aromatization was explored using two principal approaches: (i) SnCl_2/HCl reduction approach well established by Yamago and co-workers⁴³ and (ii) sodium naphthalenide reduction, in accordance with established procedures for related cycloparaphenylene systems.^{34,40} This transformation was found to be extremely sensitive to numerous experimental parameters, including temperature, concentration of the reducing agent, reaction time, oxygen exclusion and light exposure.



Scheme 2.10. Aromatization optimization big F8 double hoop.

Excess reducing equivalents consistently promoted undesired side reactions, notably acid-catalyzed rearrangements, whereas insufficient reducing agent resulted in incomplete conversion, producing mixtures of partially aromatized intermediates in which some cyclohexadiene units had undergone full aromatization to benzene while others remained intact. Optimization attempts employing freshly prepared SnCl_2/HCl in various stoichiometries induced only minor progress and even large excess of this reagent failed to achieve complete aromatization. Reaction optimizations included screening the number of equivalents of 1M sodium naphthalenide from 12–500 eqs. where employing less than 24 eqs. of reducing agent resulted in an incomplete aromatization confirmed by the presence of cyclohexadiene proton signals in the ^1H NMR spectrum as well as from mass data using MALDI-MS (Figure A2.7). An excess of reducing agent (500 eqs.) resulted in a mixture of inseparable products attributed to an over-reduction. The

reaction time was varied from 10 min to 2 h with an early quenching of the reaction provided better results. Finally, after extensive optimizations, a successful conversion was achieved by slow, dropwise addition of 36 eqs. of 1 M sodium naphthalenide solution in THF to a deoxygenated THF solution of the macrocyclic precursor maintained at $-78\text{ }^{\circ}\text{C}$. Upon addition, a rapid fluorescence color change from blue to bright green was observed, indicative of progressive aromatization. The reaction was quickly quenched within 10 min to prevent over-reduction. TLC analysis (silica) showed a bright cyan fluorescent spot ($R_f = 0.9$, 100% toluene).

Purification of the crude product using standard silica gel chromatography using toluene as eluent proved insufficient, evidenced by unresolved signals in the ^1H spectrum. After multiple attempts at purification (silica and GPC), the material was subjected to high-performance liquid chromatography (HPLC) purification. Although preliminary thin layer chromatography (TLC) and GPC analyses suggested the presence of a single species, HPLC separation revealed minor impurities. Nevertheless, the major fraction was identified as the desired **PCP-[18]CPP** nanohoop. Its structure was unequivocally confirmed by ^1H NMR and MALDI-MS (Figure A2.8-A2.9).

Competitive Study 2:

Although this achievement represented an important step forward, shortly thereafter, a competing group reported similar [2.2]PCP based lemniscular structures (Figure 2.7). Jiang et al., reported the regioselective synthesis of all-carbon 12 phenylene (6 phenylenes per loop) lemniscular carbon nanohoops *bis-po-CC* and *bis-pm-TC* through rational control of ring closures at different positions of planar chiral tetrasubstituted [2.2]paracyclophane. Topological analysis of the nanohoops confirmed that *bis-pm-TC* is topologically chiral while *bis-po-CC* is not. This distinction was visible in the CD experiments where the chiral isomers displayed opposite signals despite containing same chiral PCP core. Further, emission quantum yields for *bis-po-CC* and *bis-pm-TC* was determined to be 33% and 51%, with luminescence dissymmetry factors $|g_{\text{lum}}|$ of 1.8×10^{-3} and 3.2×10^{-3} (472 nm) respectively.⁴⁴

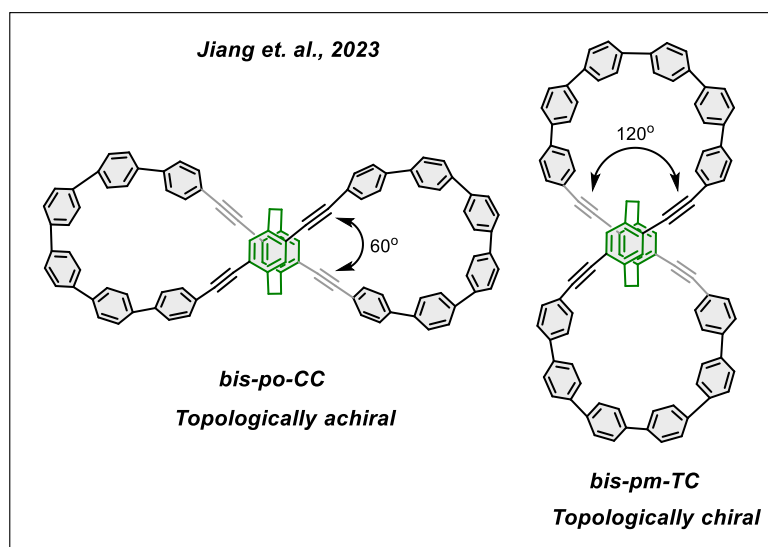
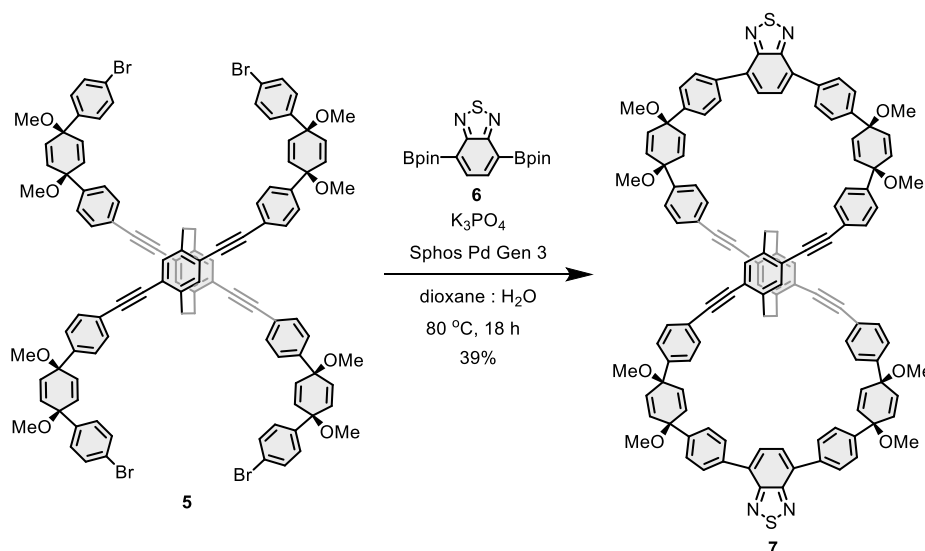


Figure 2.7. Lemniscular carbon nanohoops by Jiang group (adapted from ref⁴⁴).

Given the overlap, it became difficult to justify further development of this exact system. Nonetheless, leveraging the synthetic platform we had established, we pursued a modified design that incorporated an electron-accepting benzothiadiazole (BTD) unit. Our motivation was twofold: first, to red-shift the emission into the near-infrared (NIR) region toward red CPL emitter, and second, to understand the effect of acceptor placement on photophysical and chiroptical properties of the nanohoop.⁴⁵



Scheme 2.11. Synthesis of BTD-containing macrocycle **7**.

The BTD-containing macrocycle **7** was synthesized via a Suzuki macrocyclization reaction between previously obtained X-shaped building block **5** and BTD derivative **6** (Scheme 2.11). The desired macrocycle **7** was isolated as a yellow solid after purification by GPC, exhibiting strong green emission both in the solid state and in solution. In contrast to the previously synthesized macrocycle *pro*-PCP-[18]CPP, this macrocycle **7** could be isolated more readily as a single species, and its structure was confirmed at this stage by NMR and HRMS (Figure A2.10-A2.12).

Photophysical properties: The UV-vis absorption and emission properties were investigated for the *pro*-aromatic macrocycle **7** in toluene solutions. The macrocycle displays electronic transitions of similar energies between 300-400 nm region of the absorption spectra. Further, the macrocycle displays a green fluorescence in toluene, and the emission spectrum of the macrocycle exhibits one emission band with a maximum peak at 500 nm under excitation at 350 nm (Figure 2.8).

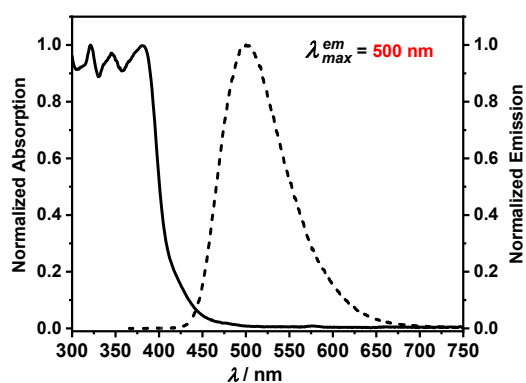
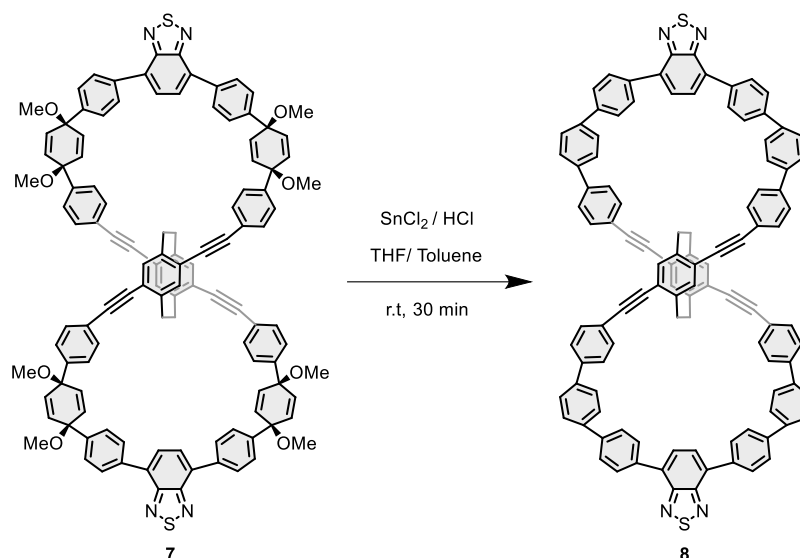


Figure 2.8. Absorption and emission spectra of **7** in toluene ($\lambda_{exc} = 350$ nm).

Aromatization: Subsequent aromatization of the macrocycle was pursued following optimized protocols established for the PCP-[18]CPP nanohoop (Scheme 2.12). Initial attempts to use sodium naphthalenide as the reducing agent were unsuccessful: even upon addition of 36 eqs. of the reagent and after 2 h of reaction, no new fluorescent product was detected. Instead, a blue-fluorescent byproduct appeared at the TLC baseline, indicating degradation via over reduction.

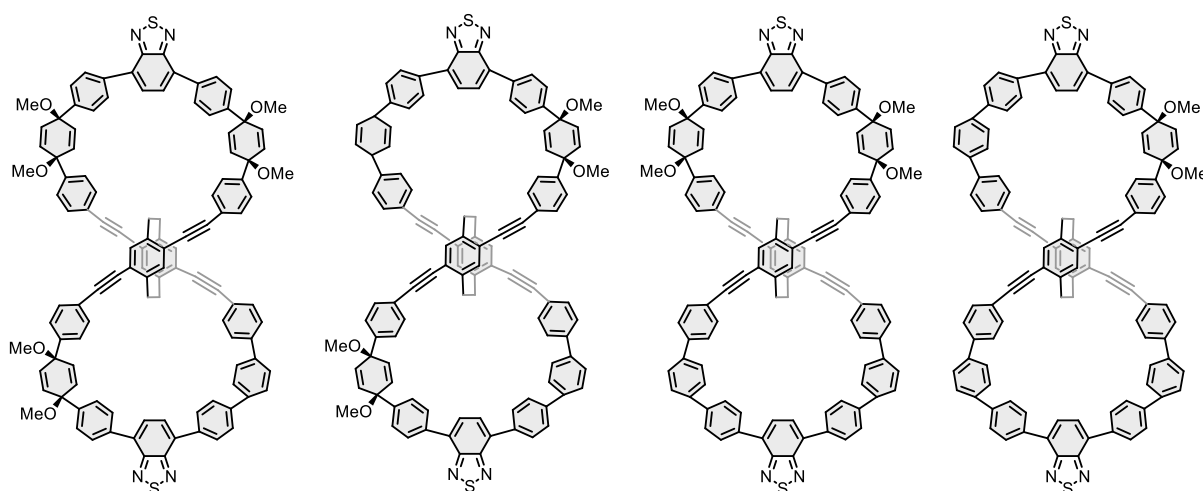


Scheme 2.12. Aromatization towards target figure-eight BTD nano hoop **8**.

To achieve milder and more controllable reaction conditions, the reduction was then attempted using SnCl_2 in presence of HCl and THF as solvent. Based on insights from prior optimizations, it was found that high concentrations of the reducing agent combined with short reaction time yielded improved outcomes, whereas low reagent concentrations and longer reaction time led to incomplete conversion and decomposition. However, excessively high reducing agent concentrations also promoted undesired acid-catalyzed rearrangements of the cyclohexadienes intermediates. Consequently, a comprehensive screening of conditions was conducted, varying the concentration of H_2SnCl_4 from 0.13 M to 0.25 M and the stoichiometry of the reducing agent from 8 to 36 eqs, trying all possible combinations of factors. Reactions at elevated temperatures ($60\text{ }^\circ\text{C}$) or in the absence of HCl were also tested, yet neither approach produced the desired product. Similarly, the use of metallic lithium (3000 eqs.) as an alternative reducing agent did not lead to product formation and the starting macrocycle was recovered as is. A similar difficulty with aromatization was reported by Harry Anderson group for porphyrin containing nano hoops, providing insights into these difficult strain-inducing aromatization reactions.⁴⁶

After extensive optimization, a successful set of conditions was identified. The desired nano hoop was obtained when 50 eqs. of concentrated H_2SnCl_4 (0.24 M) was added to a deoxygenated THF-Toluene (1:1, v/v) solution of the macrocycle **7**, with quenching after 10 min to prevent over-reduction. The reaction mixture exhibited a rapid fluorescence color change from bright green to orange-red, consistent with progressive aromatization. Thin-layer chromatography (TLC) analysis revealed the formation of an orange-red fluorescent species ($R_f = 0.6$ in 100% toluene) alongside

additional products ($R_f = 0.4-0.5$) displaying orange to yellow fluorescence. This behavior suggested a sequential, stepwise aromatization process (Scheme 2.13). Specifically, conversion of the first cyclohexadiene to a benzene unit resulted in a yellow emission visible on the TLC, while subsequent aromatization of additional cyclohexadiene moieties led to successive red-shifts in fluorescence, ultimately yielding the bright orange-red emission of the fully conjugated nano hoop. Interestingly, only this particular macrocycle **7** uniquely exhibited visible stepwise fluorescence red-shifting during aromatization.



Scheme 2.13. Possible by-products of aromatization.

However, purification of the desired nano hoop proved challenging. As expected, GPC showed a single unresolved peak, due to the similarity in the molecular sizes of the desired product and the byproducts. Silica gel column chromatography (100% toluene) afforded the target compound; however, ^1H NMR spectra indicated the presence of multiple species in small amounts. Furthermore, the nano hoop exhibited limited solubility in common organic solvents, complicating the purification and characterization. TLC analysis of the isolated product revealed that a single orange-fluorescent spot (silica TLC plate) gradually separated into multiple spots of different polarities within 2-3 min, suggesting possible post-purification degradation, consistent with the NMR-detected impurities (Figure A2.13). An additional intriguing observation was made regarding the photophysical stability of the material. Upon solvent removal, under ambient light and air, the residual solid left a pale green fluorescence in the solid state in the reaction vessel. Over time, the emission of the material in solution also evolved from orange-red to blue-white, indicating gradual photochemical degradation validating the observation during TLC analysis. To better understand this behavior, fluorescence spectra were recorded as a function of time in toluene as well as chloroform.

Photophysical behavior of nano hoop: The absorption and emission spectra of the nano hoop **8** was recorded in toluene quickly after purification and solvent removal (Figure 2.9). The absorption spectrum of **8** exhibits three major absorption peaks. Further, the nano hoop displays bright orange emission in deoxygenated toluene solution. The emission spectrum of the nano hoop exhibits one emission band with a maximum peak at 625 nm under excitation at 350 nm. It is worth noting that these emission peaks obviously shifted towards lower energy (longer wavelength) as compared to their semi-macrocycle **PCP-[7]CPP** ($\lambda_{em} = 470$ nm),³⁶ indicating an increased conjugation in **8** in addition to the effect of BTB. Slight charge transfer character was observed for nano hoop **8** with emission maximum ranging from 592 nm in cyclohexane to 634 nm in benzonitrile (Figure A2.14).

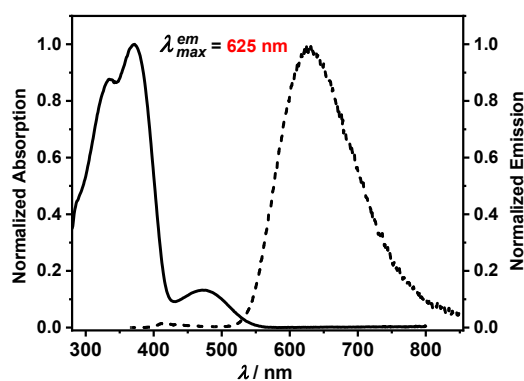


Figure 2.9. Normalized UV-vis absorption and emission spectra of **8** in toluene ($\lambda_{exc} = 350$ nm).

The emission spectra of the nano hoop in chloroform recorded over three days revealed a sudden decrease in emission intensity of the peak maximum (Figure 2.10) accompanied by a blue-shift in the emission from 630 nm to 601 nm suggesting slow decomposition of the nano hoop further validating our observations. Similar degradation was also observed in a toluene sample of the nano hoop, a decrease in emission intensity was accompanied by an appearance of a new band at around 400 nm region (Figure A2.14).

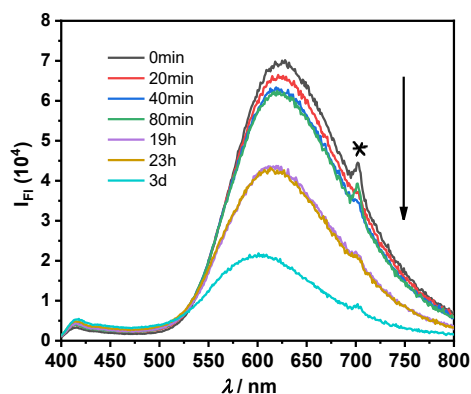


Figure 2.10. Emission spectra of **8** as a function of time in Chloroform ($\lambda_{\text{exc}} = 350 \text{ nm}$, 10^{-5} M conc) *= scattered light.

This pronounced blue-shift, accompanied by diminished intensity, reflects the intrinsic molecular instability of this large, strained conjugated chiral nanohoop. Such instability poses significant limitations for potential applications in CPL. In particular, the difficulty in isolating the individual enantiomers, combined with the rapid degradation of the material, prevents the acquisition of reliable and reproducible CPL data thus rendering this system unsuitable for practical CPL studies.

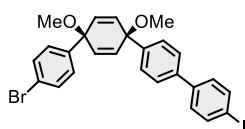
2.3 Conclusion

This chapter described the systematic design and synthesis of [2.2]paracyclophane (PCP)-based chiral carbon single and double hoops with varying size and functionality, advancing the understanding of how molecular strain and symmetry influence the chemical, photophysical and chiroptical properties. Despite significant synthetic challenges, including regioisomer control, macrocyclization efficiency and the demanding aromatization step, macrocycles were successfully synthesized and the optimized aromatization conditions developed here provide a practical route towards other highly strained conjugated macrocycles and may find applications beyond the specific systems described. Extension of this design via BTM insertion provided insight into the impact on photophysical behaviour. Although the resulting BTM-containing nanohoop exhibited promising photophysical properties with red-shifted emission, its chemical instability and poor solubility hindered detailed CPL characterization underscoring the balance between strain and molecular robustness.

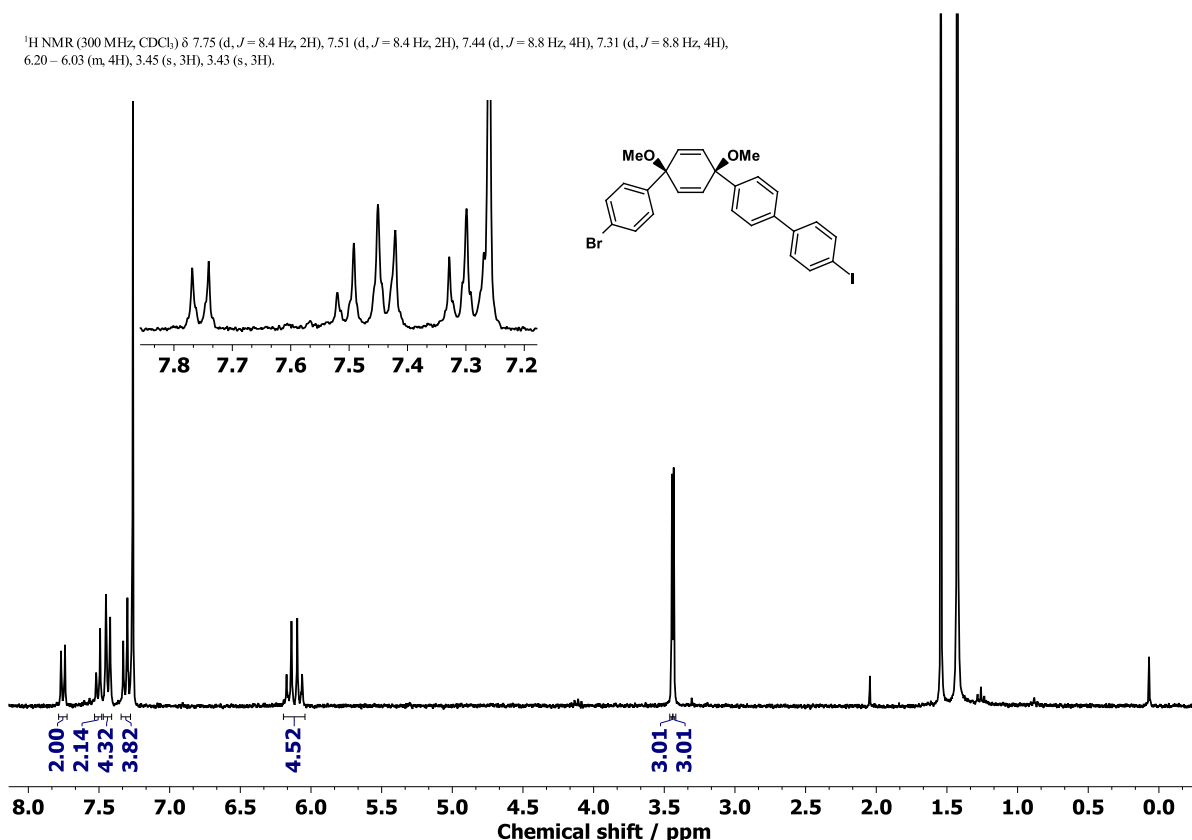
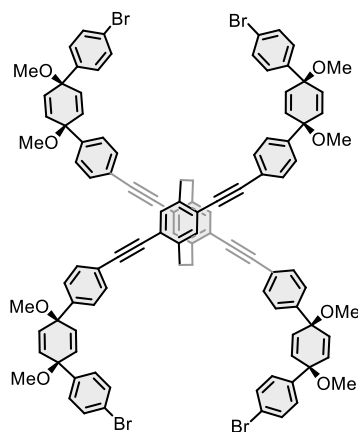
2.4 Appendix

General methods: All commercially available chemicals were purchased from Acros, Alfa Aesar, Apollo Scientific, Fluorochem and Sigma-Aldrich and used without further purification. Anhydrous solvents were purchased from Acros and stored over molecular sieves (4 Å). Column chromatography was performed on silica gel P60 (40–63 μm). TLC analysis was performed using Silica TLC plates (F254, Supelco Sigma-Aldrich™) with visualization under ultraviolet light (254 nm and 365 nm). Automated flash chromatography was performed using Biotage Isolera One. Recycling gel permeation chromatography (GPC) was performed on LaboAce 5060 from Japan Analytical Industry using JAIGEL-2HR Plus (20×600 mm, two columns in series) as columns, and an appropriate solvent. For preparative HPLC, a Shimadzu LC-20AP HPLC was used equipped with a diode-array UV/Vis detector (SPD-M20 A VP from Shimadzu, λ=200–600 nm). NMR experiments were performed at ambient temperature using a Bruker AV II and III NMR spectrometers operating at 300, 400, or 500 MHz proton frequencies. The instruments were equipped with a direct-observe 5 mm BBFO smart probe (400 and 500 MHz). All probes were equipped with actively shielded z-gradients (10 Å). The chemical shifts are reported in ppm relative to tetramethylsilane or referenced to residual solvent peak and the J values are given in Hz (±0.1 Hz). High resolution mass spectra (HRMS, FD+) were collected on an AccuTOF LC, JMS-T100LP Mass spectrometer (JEOL, Japan). UV-vis absorption was recorded on the spectrophotometer Shimadzu UV2700 equipped with a deuterium lamp (190–350 nm), a halogen lamp (330–900 nm) and a photomultiplier (Hamamatsu R928). Emission spectra were recorded with Horiba Jobin Vyon Fluorolog-3 spectrofluorometer in an appropriate solvent in 1.0 cm cuvette. Compounds **1a-c**,^{12,13,47} **1d-g**,³⁹ **3a-c**^{34,40–42} were synthesized according to reported protocols, and the spectral data matches with the literature.

Synthesis of 4a:



Ketone **2b** (5 g, 17.9 mmol, 1 eq) and diiodobiphenyl (7.6 g, 18.8 mmol, 1.05 eq) weighed in separate dry flasks and 55 ml and 300 ml of dry THF was added to both flasks, respectively. The solution of diiodobiphenyl was kept at –78 °C and *n*-BuLi (7.8 ml, 19.7 mmol, 1.1 eq, 2.5 M) was dropwise added over 30 min and stirred for 1 h. To this solution, the solution of ketone (stirred at –78 °C for 1 h) was cannulated. The reaction was stirred for 2 h at this temperature and slowly warmed to room temperature. The reaction was quenched with water and crude was extracted with ethyl acetate three times. The organic layers were combined, and solvents were removed under vacuo. The crude was further dissolved in 50 ml dry THF and cooled to 0 °C. NaH (60% dispersion in mineral oil 1.43 g, 35.8 mmol, 2 eq) was added and mixture was stirred for 30 min followed by addition of iodomethane (5.5 ml, 5 eq). The reaction was stirred overnight and quenched with water followed by extraction with ethyl acetate. The product was washed with brine, dried over sodium sulfate and solvents were removed under vacuo. The product (cis **4a**) was isolated using flash column chromatography (3% EA-CH) as an off-white solid (1.3 g, 12.7%).

Figure A2.1. ¹H NMR of **4a** in CDCl₃.Synthesis of **5**:

In a dry Schlenk flask, **1g** (40 mg, 0.13 mmol, 1 eq), **3b** (390 mg, 0.79 mmol, 6 eq), CuI (10 mg, 53 μmol, 0.4 eq), PPh₃ (28 mg, 0.11 mmol, 0.8 eq) and Pd₂dba₃ (24 mg, 26 μmol, 0.2 eq) were added, and the flask was evacuated and backfilled with argon three times. Then at 0°C, dry THF (5 ml) and TEA (1.35 ml) were added, and the reaction was warmed to room temperature and monitored at this temperature via TLC until completion. The crude mixture was passed through celite and extracted with dichloromethane three times. The solvents were removed under vacuo. The product was dissolved in minimum amount of dichloromethane and pentane was added to form precipitates. The residue was filtered, washed with pentane and the precipitates were dried in vacuo. The crude mixture was purified by GPC in Chloroform as a yellow solid (100 mg, 43%). ¹H NMR (300 MHz, CDCl₃, 298 K, δ/ppm): 7.55 (d, *J* = 8.3 Hz, 8H), 7.47 (d, *J* = 8.5 Hz, 8H), 7.42 (d, *J* = 8.4 Hz, 8H), 7.31 (d, *J* = 8.5 Hz, 8H), 7.14 (s, 4H), 6.19 – 6.08 (m, 16H), 3.71 – 3.51 (m, 4H), 3.46 (s, 12H), 3.45 (s, 12H), 3.21 – 3.00 (m, 4H). ¹³C NMR (75 MHz, CDCl₃) δ 143.52, 142.50, 142.04, 134.64, 133.52, 133.42, 133.37, 133.28, 131.67, 131.57, 127.87, 126.21, 125.11, 122.99, 121.76, 94.44, 89.54, 74.71, 74.52, 52.10, 32.76. HRMS (ESI, +): *m/z* calcd. for C₁₀₄H₈₄Br₄O₈Na [M+Na]⁺: 1799.2792, found: 1799.2802.

^1H NMR (300 MHz, CDCl_3) δ 7.55 (d, $J = 8.3$ Hz, 8H), 7.47 (d, $J = 8.5$ Hz, 8H), 7.42 (d, $J = 8.4$ Hz, 8H), 7.31 (d, $J = 8.5$ Hz, 8H), 7.14 (s, 4H), 6.19 – 6.08 (m, 16H), 3.71 – 3.51 (m, 4H), 3.46 (s, 12H), 3.45 (s, 12H), 3.21 – 3.00 (m, 4H).

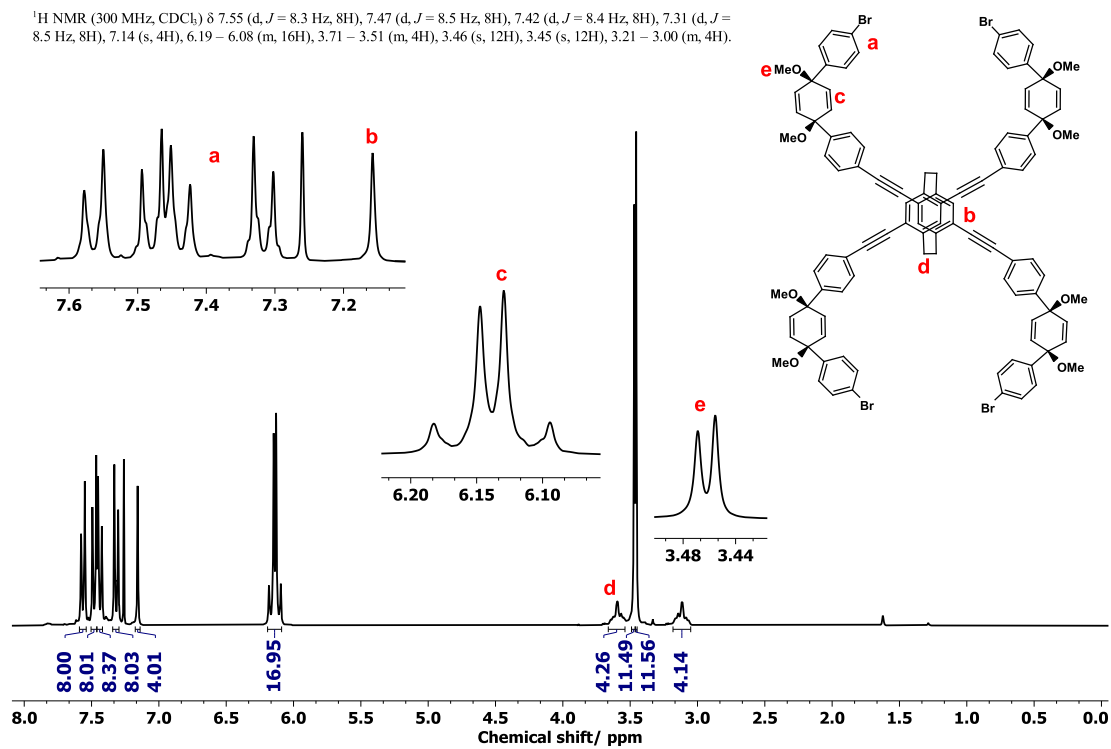


Figure A2.2. ^1H NMR of **5** in CDCl_3 .

^{13}C NMR (75 MHz, CDCl_3) δ 143.52, 142.50, 142.04, 134.64, 133.52, 133.42, 133.37, 133.28, 131.67, 131.57, 127.87, 126.21, 125.11, 122.99, 121.76, 94.44, 89.54, 74.71, 74.52, 52.10, 32.76.

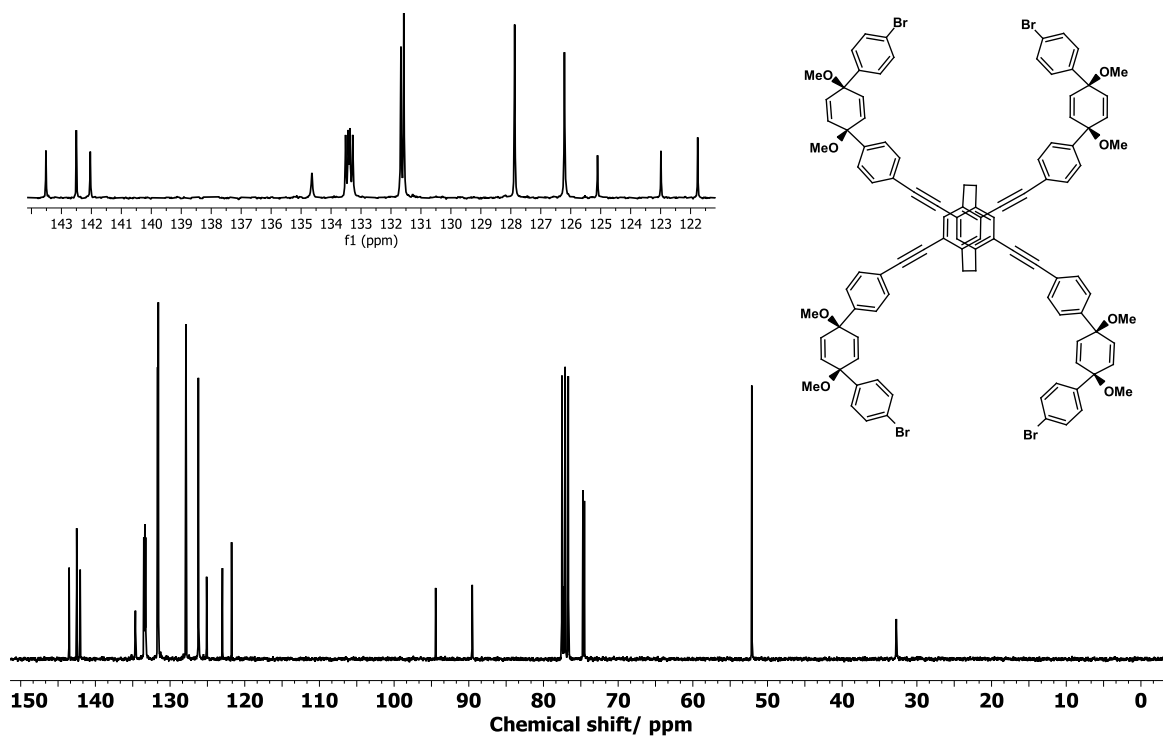
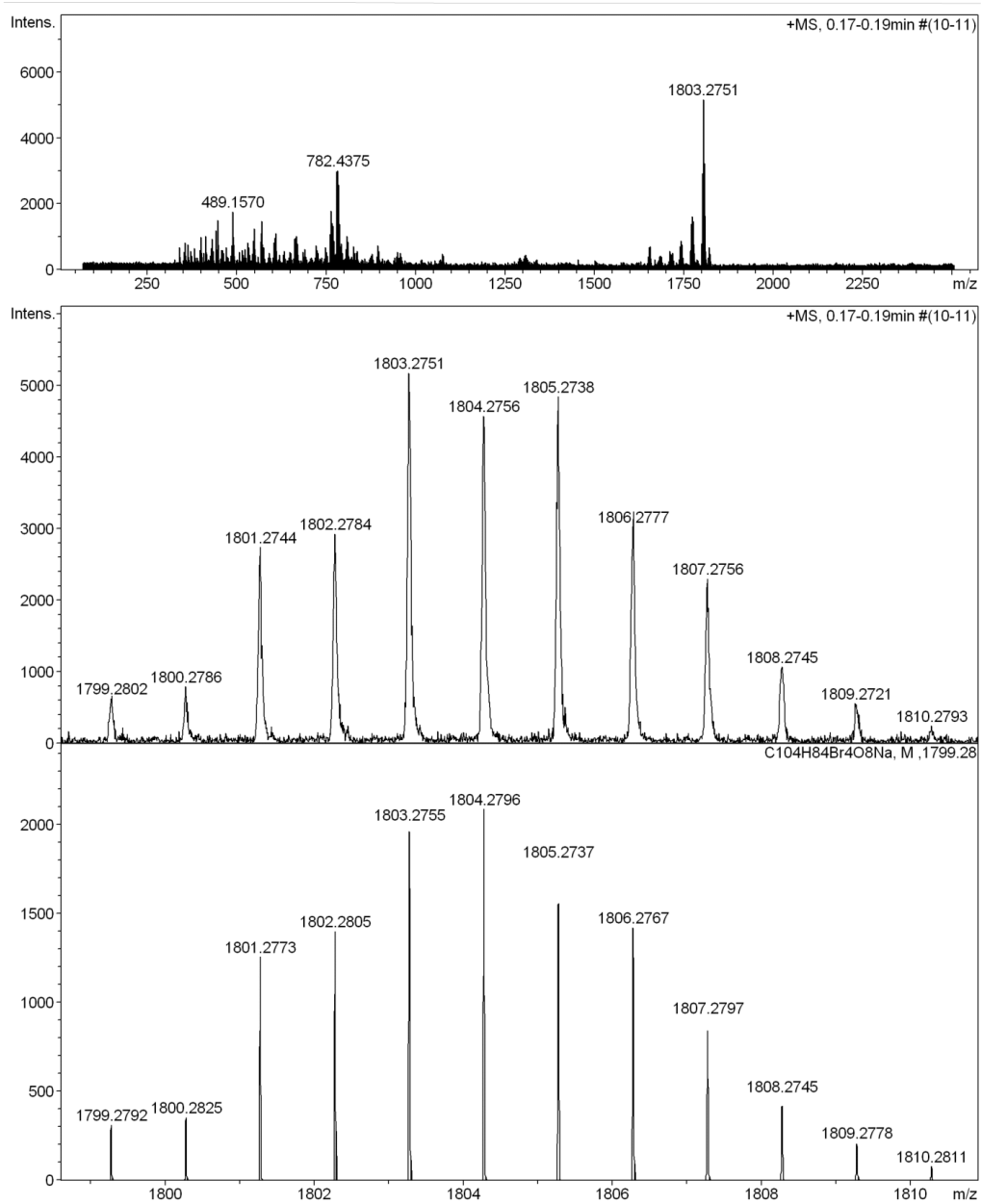


Figure A2.3. ^{13}C NMR of **5** in CDCl_3 .

High Resolution Mass Spectrometry Report

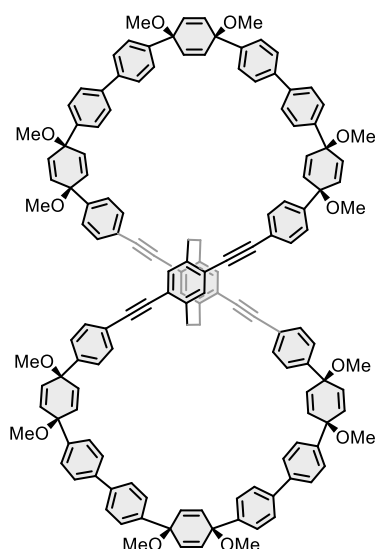
Sample Name **precursor**
CommentInstrument maXis 4G
Method 24 Direct_pos_high.m

Bruker Compass DataAnalysis 4.0

Acquisition Date 06.10.2022 14:32:11

Page 1 of 3

Figure A2.4. HRMS (ESI,+) spectrum of 5 [M+Na]⁺.

Synthesis of *pro*-PCP-[18]CPP:

Under argon, 1,4-dioxane (1.5 ml) was added to the mixture of **5** (30 mg, 17 μmol , 1 eq) and **3c** (18 mg, 34 μmol , 2 eq) and deoxygenated for 30 min. Afterwards, SPhos Pd Gen III (14 mg, 19 μmol , 1.1 eq) was added and the bubbling was continued for another 15 min. The reaction vessel was placed in a pre-heated oil bath at 80 $^{\circ}\text{C}$ for 10 min, and 0.15 ml of 2M K_3PO_4 was added. The temperature was increased to 105 $^{\circ}\text{C}$ and reaction was allowed to run at this temperature for 2 days. After completion of the reaction, the crude was extracted with dichloromethane and solvents were removed under vacuo. The crude was further passed through silica and introduced to GPC for further purification. The desired macrocycle was obtained as a possible mixture of isomers and used without further purification after confirmation by mass spectrometry and ^1H NMR displaying proton signals in the expected region.

HRMS (ESI, +): m/z calcd. for $\text{C}_{144}\text{H}_{120}\text{O}_{12}\text{Na}$ $[\text{M}+\text{Na}]^+$: 2063.8672, found: 2063.8670.

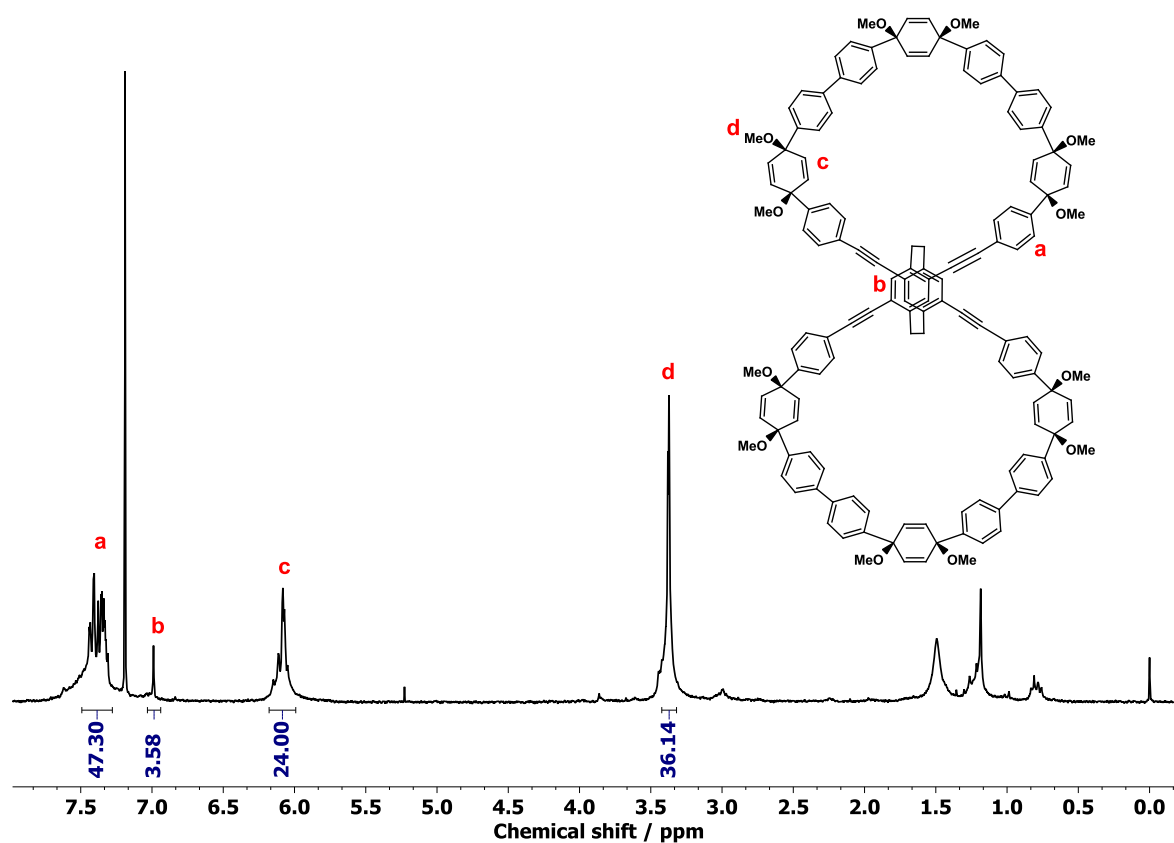
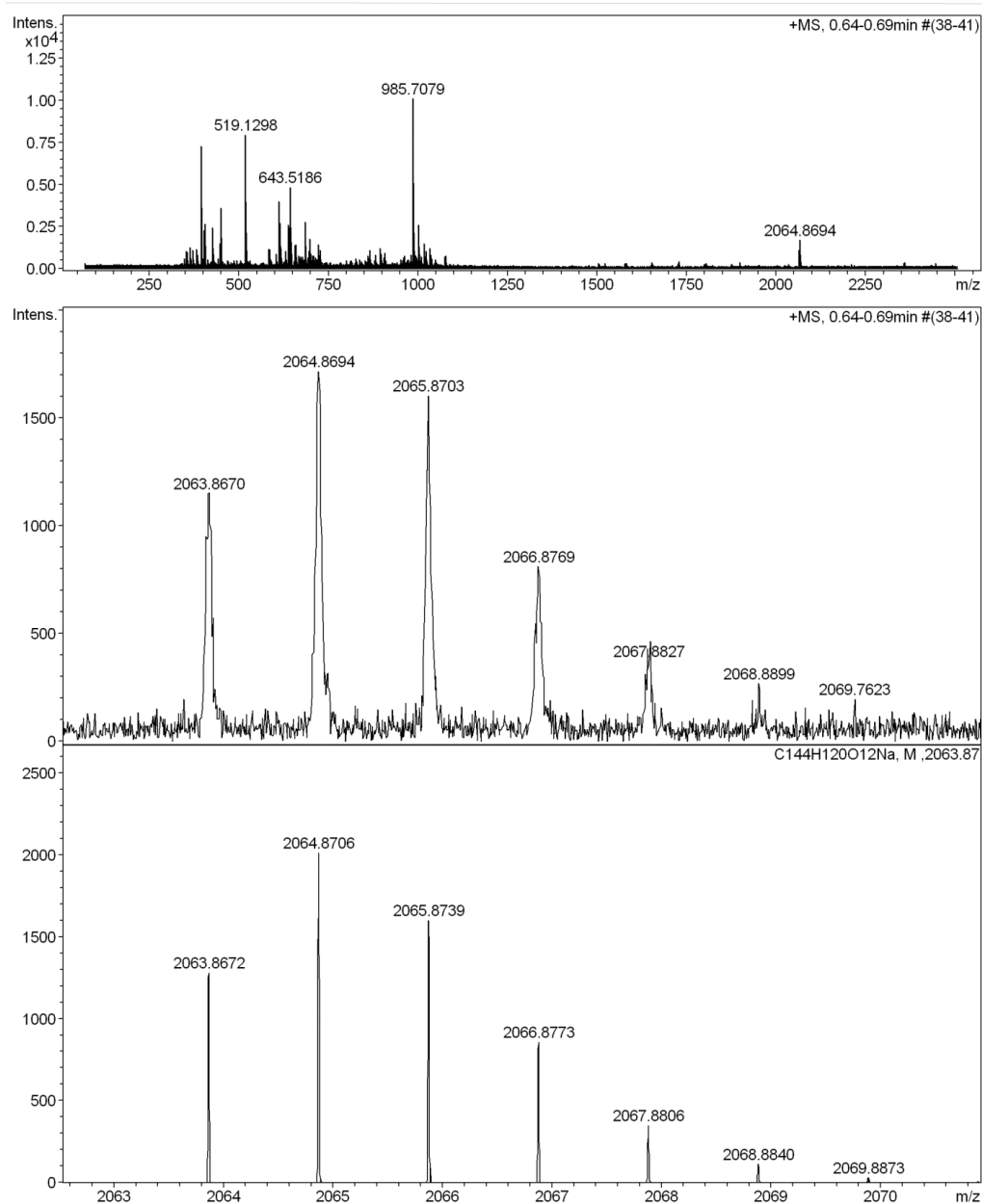


Figure A2.5. ^1H NMR of *pro*-PCP-[18]CPP in CDCl_3 .

High Resolution Mass Spectrometry Report

Sample Name **macrocycle**
CommentInstrument maXis 4G
Method 24 Direct_pos_high.m

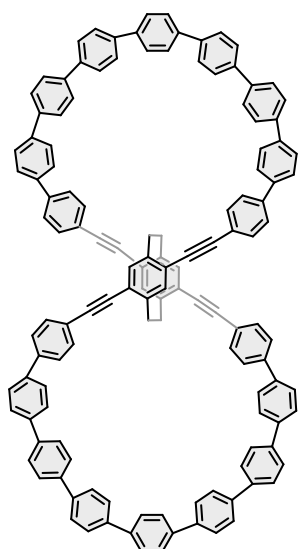
Bruker Compass DataAnalysis 4.0

Acquisition Date 06.10.2022 14:33:29

Page 1 of 3

Figure A2.6. HRMS (ESI,+) spectrum of *pro*-PCP-[18]CPP [M+Na]⁺.

Synthesis of PCP-[18]CPP:



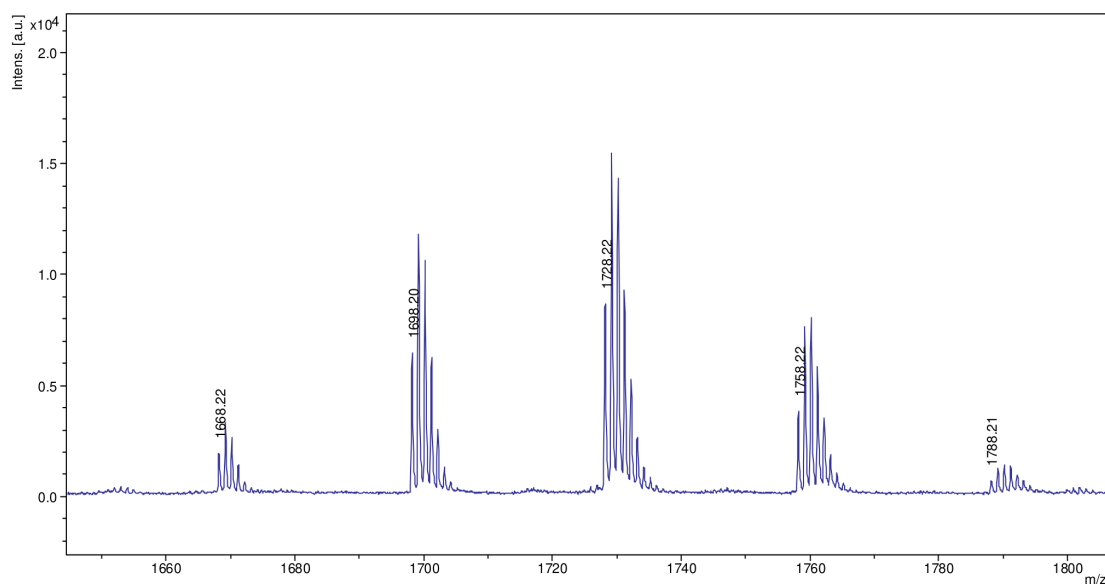
To an oven-dried flask, naphthalene (473 mg, 3.8 mmol) was added in 3.8 ml dry THF. To this solution, sodium (125 mg, 5.56 mmol) was added under argon, and the reaction mixture was ran for 18 h at room temperature. A green solution containing sodium naphthalenide was formed. To a solution of *pro*-PCP-[18]CPP (40 mg, 20 μ mol, 1 eq) in 3 ml THF, sodium naphthalenide (0.72 ml, 1M, 36 eq) was added at -78°C . The reaction was stirred at this temperature for 10 min and iodine (1 ml, 1M solution in THF) was added. A sudden blue-green fluorescence was observed in the reaction. The solution was warmed to room temperature and aqueous sodium thiosulfate solution was carefully added to remove excess I_2 . The crude mixture was extracted with ethyl acetate three times. The solvents were removed under vacuo and crude was dried. Purification was performed using silica gel chromatography in 100% toluene (product $R_f = 0.9$). Further

purification was performed using preparative HPLC using a mixture of eluents (EA-PE : 40-60) to afford the desired nanohoop (7mg, 20%). **HRMS (MALDI, +, DCTB matrix):** m/z calcd. for $\text{C}_{132}\text{H}_{84} [\text{M}]^+$: 1668.6568, found: 1668.6562.

D:\MALDI Data\DCBP\Solomek\Kovida KS051 DCTB RP a\0_L9\1\1SRef

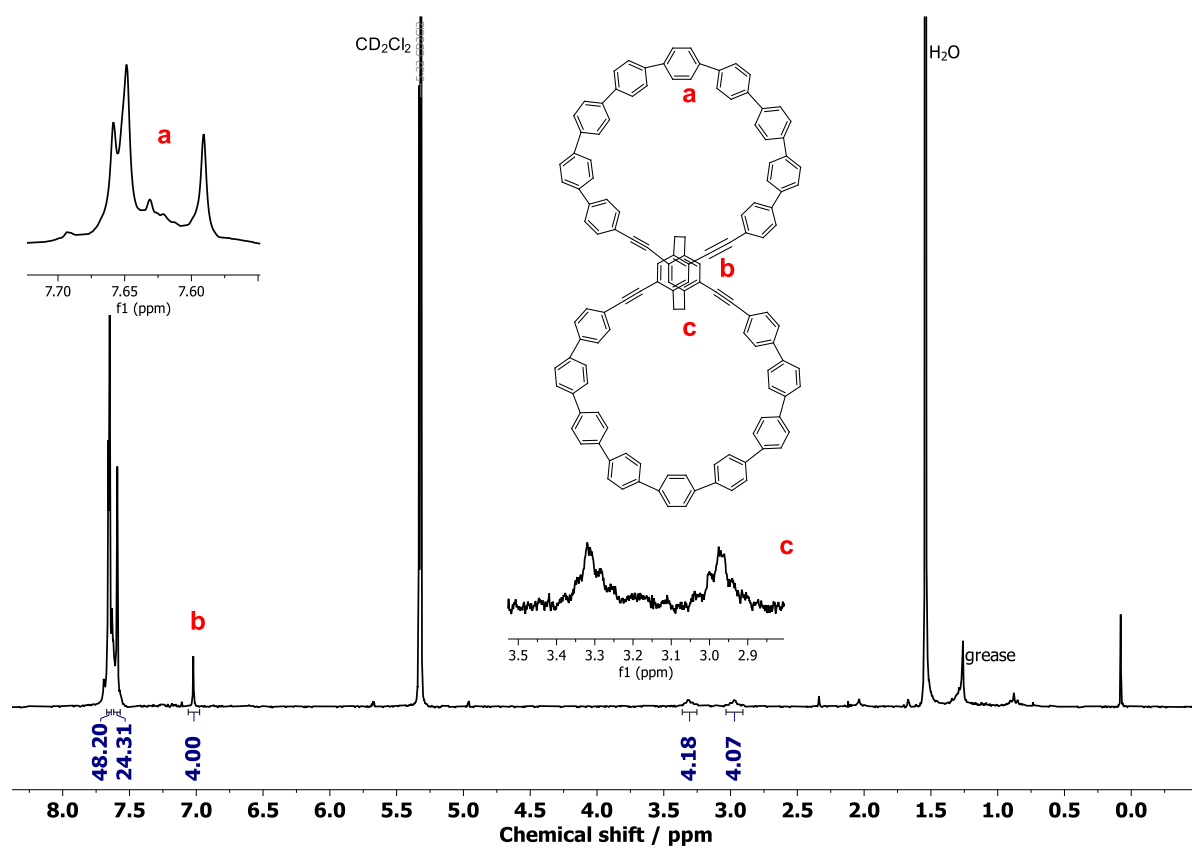
Comment 1 Kovida KS051 DCTB RP a

Comment 2 Kovida KS051 DCTB RP a



printed: 7/27/2022 10:24:28

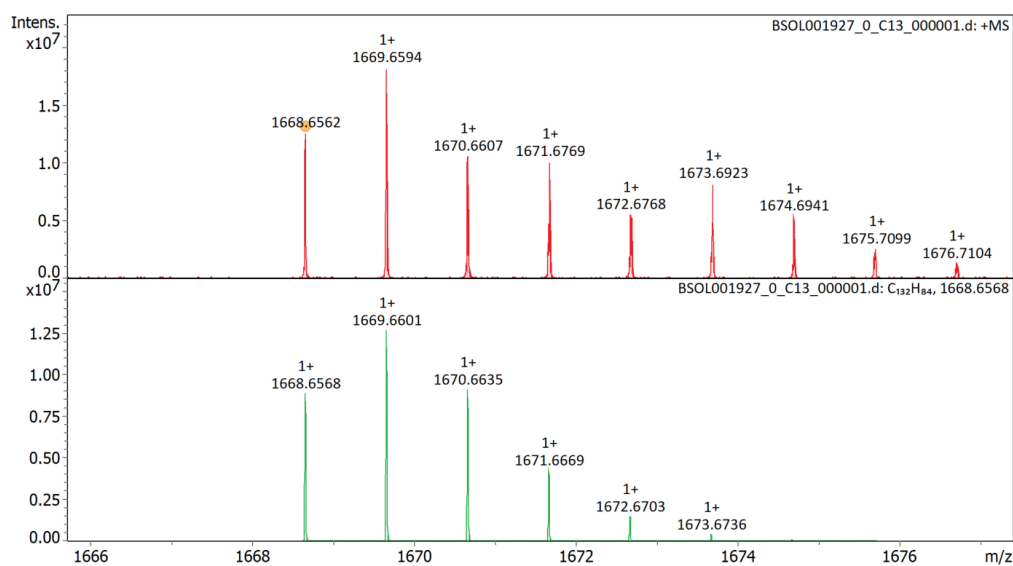
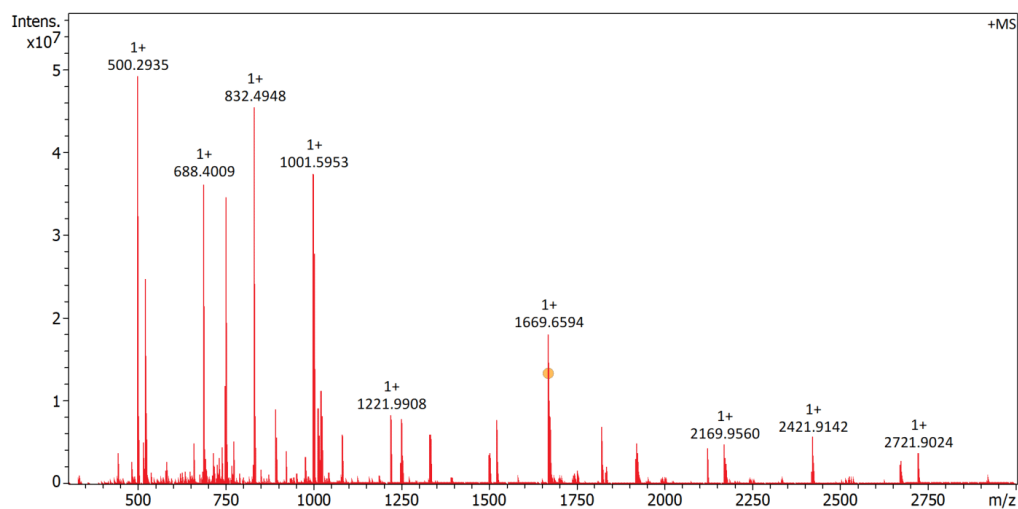
Figure A2.7. MALDI spectrum of PCP-[18]CPP during reaction optimizations.

Figure A2.8. ^1H NMR of PCP-[18]CPP in CD_2Cl_2 .

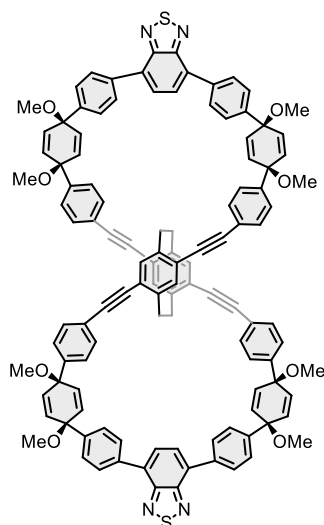
BSOL001927 Juraj Malincik/ - KS-036_F1 - DCM - DCTB 1:10

Acquisition Parameter

Method:	MALDI_MS_POS_300-3000_2M_16AvScans	Acquisition Date:	14.12.2022 10:23:44		
File Name:	D:\Data\ETH Data\BSOL0019xx\BSOL001927_0_C13_000001.d	Operator:	Louis Bertschi		
Source	Dual (MALDI/ESI)	Polarity	Positive	Nebulizer Gas	1.0 bar
Broadband Low Mass	303.1 m/z	Laser Power	25.8 lp	Drying Gas Flow Rate	4.0 L/min
Broadband High Mass	3000.0 m/z			Capillary	2800.0 V
No. of Cell Fills	1	Time of Flight to Detector	0.002 sec	Drying Gas Temperature	200.0 °C
Apodization	Full-Sine				

**Figure A2.9.** HRMS (MALDI, +) spectrum of **PCP-[18]CPP**.

Synthesis of 7:



To a Schlenk flask, **5** (40 mg, 22 μmol , 1 eq), **6** (19 mg, 49 μmol , 2.2 eq) and SPhos Pd Gen III (8.8 mg, 11 μmol , 0.5 eq) were added and the flask was evacuated and back filled with argon three times. To the combined solids, 8 ml deoxygenated 1,4-dioxane (bubbled with argon for 1 h) and bubbling was continued for another 15 min. The flask was placed in a pre-heated oil bath set at 80 $^{\circ}\text{C}$ and 1 ml aqueous K_3PO_4 solution (2M) was dropwise added to the reaction mixture while stirring. The reaction flask was heated at this temperature for 18 h and reaction was monitored using TLC. After the completion of the reaction, crude product was extracted with dichloromethane and solvents were removed under vacuo and product was dried. The crude was purified using silica gel chromatography (30% EA-PE) followed by GPC (chloroform) to afford the desired product as a yellow solid

(15 mg, 39%) with bright green fluorescence in both solid state and solution. $^1\text{H NMR}$ (300 MHz, CDCl_3 , 298 K, δ/ppm): 7.89 (d, $J = 8.4$ Hz, 8H), 7.77 (s, 4H), 7.52 (d, $J = 8.4$ Hz, 8H), 7.35 (d, $J = 8.5$ Hz, 8H), 7.22 (d, $J = 8.4$ Hz, 8H), 6.76 (s, 4H), 6.40 – 6.25 (m, 8H), 6.11 (d, $J = 10.5$ Hz, 8H), 3.52 (s, 12H), 3.51 – 3.47 (m, 4H), 3.44 (s, 12H), 3.14 – 2.85 (m, 4H). $^{13}\text{C NMR}$ (75 MHz, CDCl_3 , 298 K, δ/ppm): 154.27, 143.28, 142.96, 142.43, 137.19, 134.04, 133.84, 133.20, 133.01, 132.85, 132.66, 131.51, 129.26, 128.62, 126.55, 126.41, 123.97, 122.67, 95.23, 89.44, 75.46, 75.25, 52.36, 51.91, 33.20. **HRMS (ESI, +)**: m/z calcd. for $\text{C}_{116}\text{H}_{88}\text{N}_4\text{O}_8\text{S}_2\text{Na}$ $[\text{M}+\text{Na}]^+$: 1752.5968, found: 1752.5699.

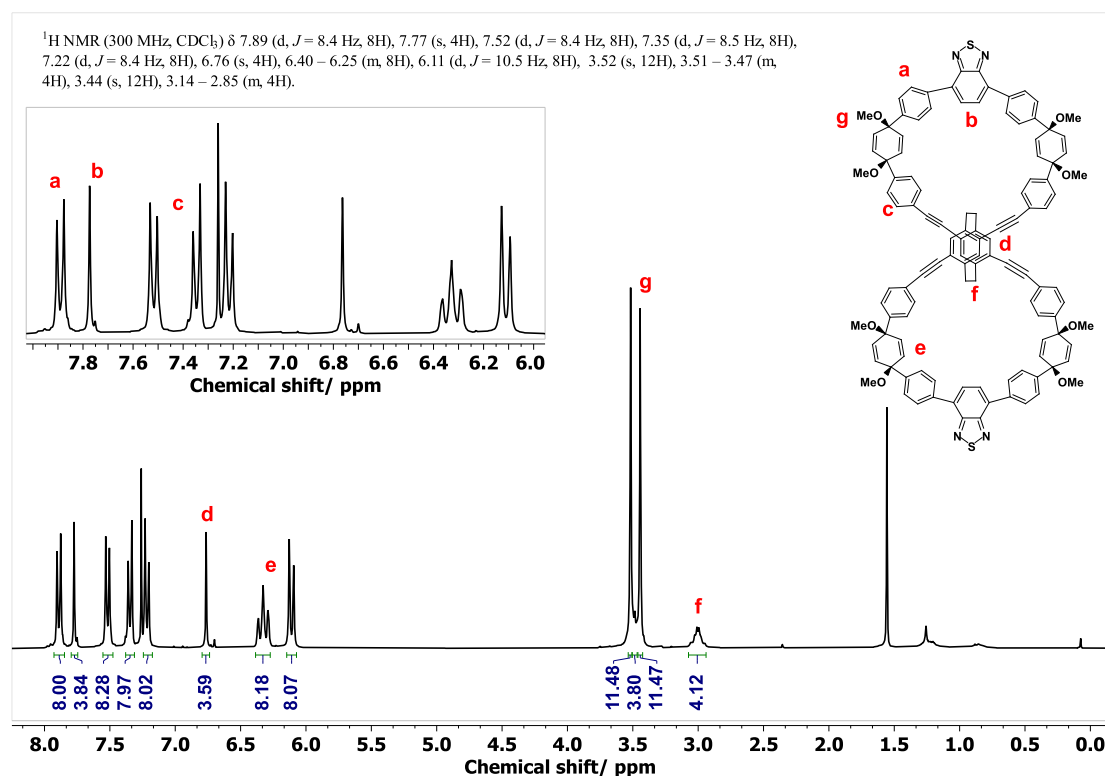
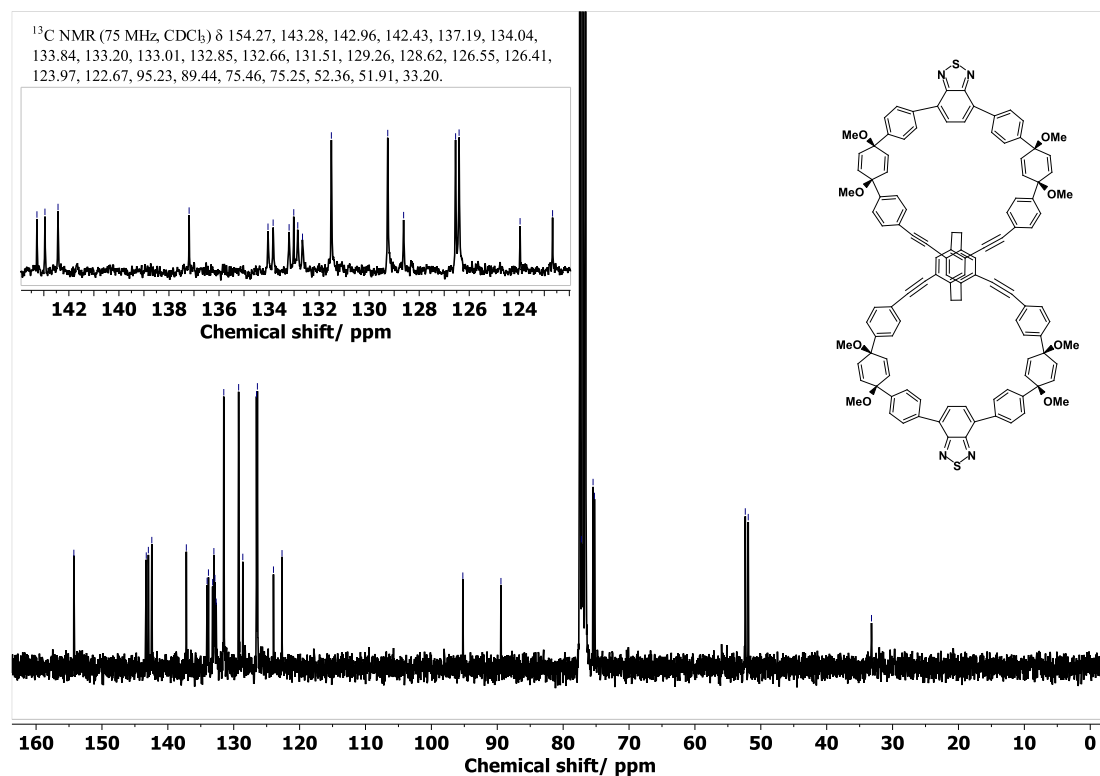
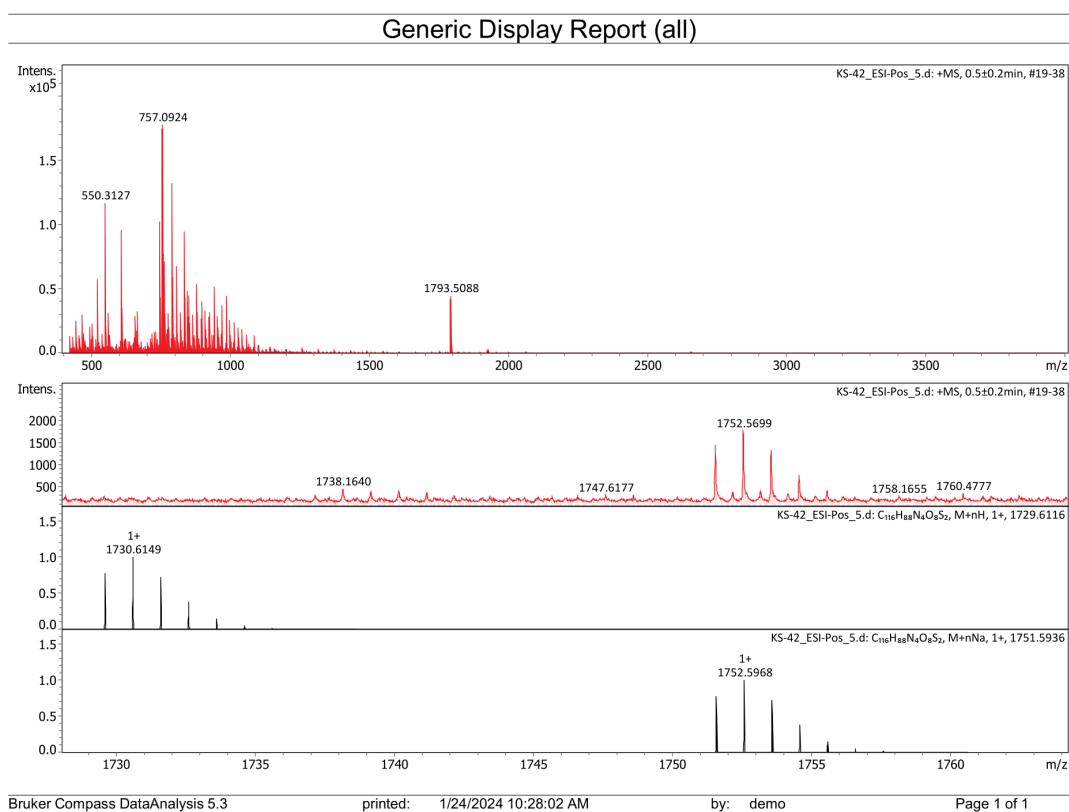
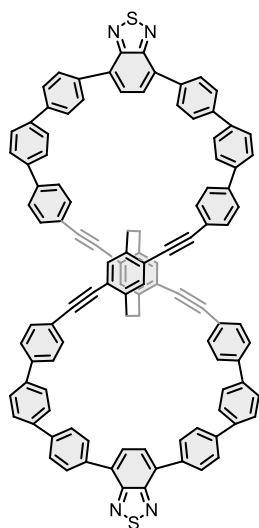


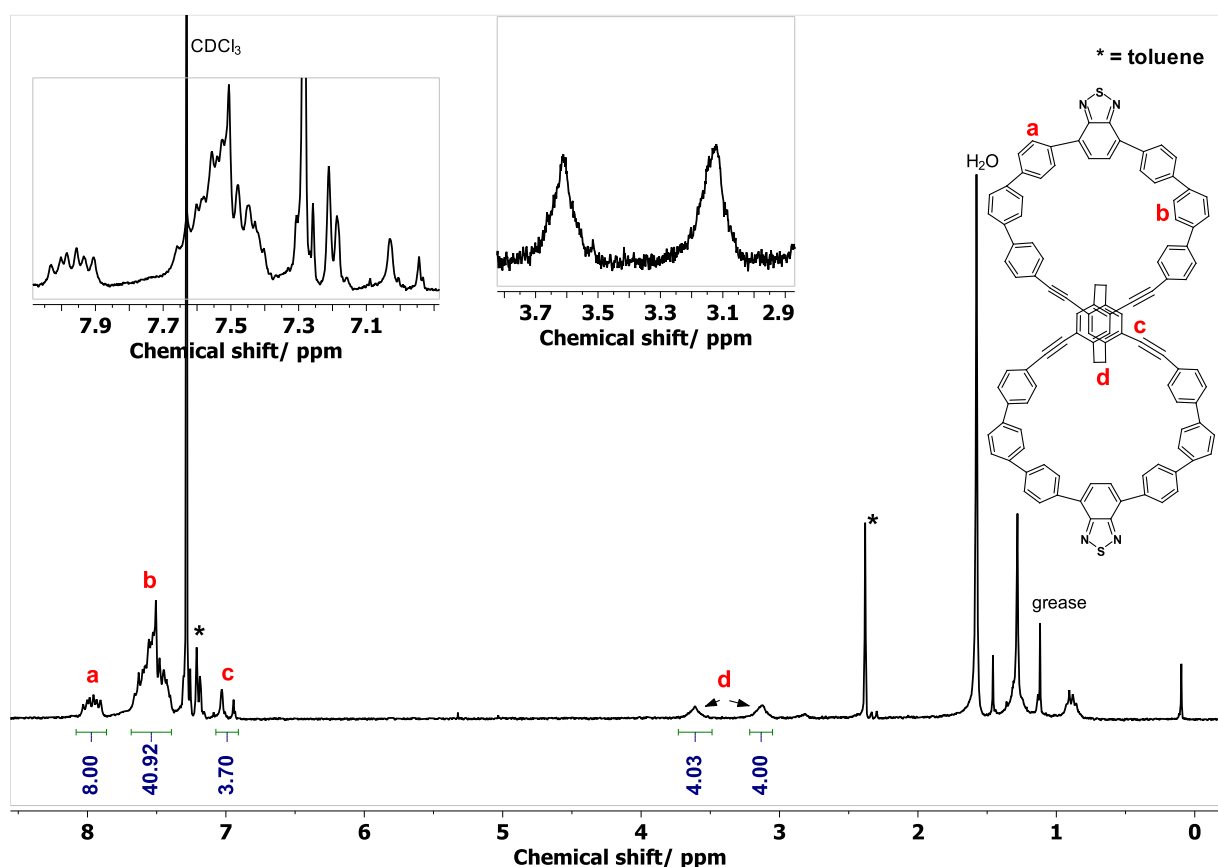
Figure A2.10. $^1\text{H NMR}$ of **7** in CDCl_3 .

Figure A2.11. ^{13}C NMR of 7 in CDCl_3 .Figure A2.12. HRMS (ESI, +) spectrum of 7 $[\text{M}+\text{Na}]^+$.

Synthesis of 8:



To a dry flask, **7** (20 mg, 12 μmol , 1 eq) was dissolved in 2.5 ml THF and 2.5 ml toluene and the solution was deoxygenated using argon for 30 min. A solution of H_2SnCl_4 was freshly prepared by adding $\text{SnCl}_2 \cdot 2\text{H}_2\text{O}$ (270 mg), and 0.2 ml HCl to 5 ml THF and deoxygenating for 30 min. 2.4 ml of this solution was added the solution of **7** in THF. A sudden change in fluorescence from bright green to bright red was observed in the reaction vessel and solution becomes clear after 20 min. The reaction was quenched after 30 min, using an aqueous NaOH solution (1M). The crude product was extracted using dichloromethane, organic layers were combined, and solvents were removed under vacuo and product was dried. The crude was purified using silica gel chromatography (100% toluene) followed by GPC (chloroform) to afford the desired product as a red solid (5 mg, 30%) with bright orange-red fluorescence in both solid state and solution. No mass was observed for the nano hoop in ESI. MALDI was not performed on this sample.



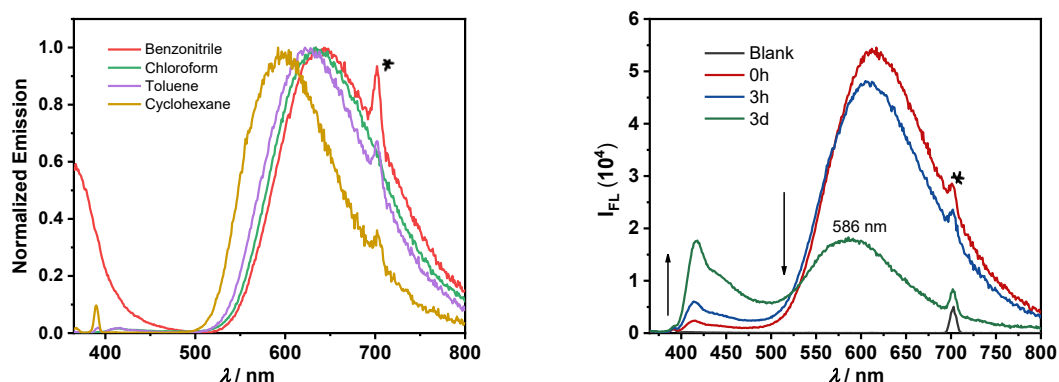


Figure A2.14. Normalized emission spectra of **8** in different solvents (left image, $\lambda_{\text{exc}} = 350$ nm) and emission spectra of **8** recorded over time in toluene (right image, $\lambda_{\text{exc}} = 350$ nm, 10^{-5} M conc) *= scattered light.

2.5 References

- (1) Hassan, Z.; Zysman-Colman, E.; Lahann, J.; Bräse, S. From Molecules to Materials: Collaborative Research at the Chemistry—Materials Science Interface and Lessons Learned in Cyclophane Chemistry. *Adv. Funct. Mater.* **2024**, *34* (47), 2403365. <https://doi.org/10.1002/adfm.202403365>.
- (2) Hassan, Z. Molecular Insights into [2.2]Paracyclophane-Based Functional Materials: Chemical Aspects Behind Functions. *Adv. Funct. Mater.* **2024**, *34* (47), 2311828. <https://doi.org/10.1002/adfm.202311828>.
- (3) Hassan, Z.; Spuling, E.; Knoll, D. M.; Bräse, S. Regioselective Functionalization of [2.2]Paracyclophanes: Recent Synthetic Progress and Perspectives. *Angew. Chem. Int. Ed.* **2020**, *59* (6), 2156–2170. <https://doi.org/10.1002/anie.201904863>.
- (4) Elacqua, E.; MacGillivray, L. R. From the Decks to the Bridges: Optoelectronics in [2.2]Paracyclophane Chemistry. *Eur. J. Org. Chem.* **2010**, *2010* (36), 6883–6894. <https://doi.org/10.1002/ejoc.201000930>.
- (5) Lambud, S.; Bhadke, A.; Siddiqui, Z. A.; Chaudhari, V.; Sekar, N.; Bhosale, R.; More, S. Synthesis and Optical Property Modulation of Substituted [2.2]Paracyclophanes through Through-Space Conjugation. *Eur. J. Org. Chem.* **2024**, *27* (25), e202400360. <https://doi.org/10.1002/ejoc.202400360>.
- (6) Morisaki, Y.; Chujo, Y. Through-Space Conjugated Polymers Consisting of [2.2]Paracyclophane. *Polym. Chem.* **2011**, *2* (6), 1249. <https://doi.org/10.1039/c0py00421a>.
- (7) Zafra, J. L.; Molina Ontoria, A.; Mayorga Burrezo, P.; Peña-Alvarez, M.; Samoc, M.; Szeremeta, J.; Ramírez, F. J.; Lovander, M. D.; Droske, C. J.; Pappenfus, T. M.; Echegoyen, L.; López Navarrete, J. T.; Martín, N.; Casado, J. Fingerprints of Through-Bond and Through-Space Exciton and Charge π -Electron Delocalization in Linearly Extended [2.2]Paracyclophanes. *J. Am. Chem. Soc.* **2017**, *139* (8), 3095–3105. <https://doi.org/10.1021/jacs.6b12520>.
- (8) Xu, Y.; Hafeez, H.; Seibert, J.; Wu, S.; Ortiz, J. S. O.; Crassous, J.; Bräse, S.; Samuel, I. D. W.; Zysman-Colman, E. [2.2]Paracyclophane-Substituted Chiral Multiresonant Thermally Activated Delayed Fluorescence Emitters for Efficient Organic Light-Emitting Diodes. *Adv. Funct. Mater.* **2024**, *34* (47), 2402036. <https://doi.org/10.1002/adfm.202402036>.
- (9) Felder, S.; Wu, S.; Brom, J.; Micouin, L.; Benedetti, E. Enantiopure Planar Chiral [2.2]Paracyclophanes: Synthesis and Applications in Asymmetric Organocatalysis. *Chirality* **2021**, *33* (9), 506–527. <https://doi.org/10.1002/chir.23335>.
- (10) Morisaki, Y.; Gon, M.; Chujo, Y. Conjugated Microporous Polymers Consisting of Tetrasubstituted [2.2]Paracyclophane Junctions. *J. Polym. Sci. Part Polym. Chem.* **2013**, *51* (10), 2311–2316. <https://doi.org/10.1002/pola.26600>.
- (11) Spuling, E.; Sharma, N.; Samuel, I. D. W.; Zysman-Colman, E.; Bräse, S. (Deep) Blue through-Space Conjugated TADF Emitters Based on [2.2]Paracyclophanes. *Chem. Commun.* **2018**, *54* (67), 9278–9281. <https://doi.org/10.1039/C8CC04594A>.
- (12) Meyer-Eppler, G.; Sure, R.; Schneider, A.; Schnakenburg, G.; Grimme, S.; Lützen, A. Synthesis, Chiral Resolution, and Absolute Configuration of Dissymmetric 4,15-Difunctionalized [2.2]Paracyclophanes. *J. Org. Chem.* **2014**, *79* (14), 6679–6687. <https://doi.org/10.1021/jo501212t>.

- (13) Bondarenko, L.; Dix, I.; Hinrichs, H.; Hopf, H. Cyclophanes. Part LII: Ethynyl[2.2]Paracyclophanes - New Building Blocks for Molecular Scaffolding. *Synthesis* **2004**, *2004* (16), 2751–2759. <https://doi.org/10.1055/s-2004-834872>.
- (14) Reich, H. J.; Cram, D. J. Macro Rings. XXXVII. Multiple Electrophilic Substitution Reactions of [2.2]Paracyclophanes and Interconversions of Polysubstituted Derivatives. *J. Am. Chem. Soc.* **1969**, *91* (13), 3527–3533. <https://doi.org/10.1021/ja01041a017>.
- (15) Kikuchi, K.; Nakamura, J.; Nagata, Y.; Tsuchida, H.; Kakuta, T.; Ogoshi, T.; Morisaki, Y. Control of Circularly Polarized Luminescence by Orientation of Stacked π -Electron Systems. *Chem. – Asian J.* **2019**, *14* (10), 1681–1685. <https://doi.org/10.1002/asia.201801741>.
- (16) Reznikova, K.; Hsu, C.; Schosser, W. M.; Gallego, A.; Beltako, K.; Pauly, F.; van der Zant, H. S. J.; Mayor, M. Substitution Pattern Controlled Quantum Interference in [2.2]Paracyclophane-Based Single-Molecule Junctions. *J. Am. Chem. Soc.* **2021**, *143* (34), 13944–13951. <https://doi.org/10.1021/jacs.1c06966>.
- (17) Yanagawa, A.; Inoue, R.; Morisaki, Y. Synthesis and Characterization of One-Handed Helical Oligo(*o*-Phenylene)s: Control of Axial Chirality by Planar Chiral [2.2]Paracyclophane. *Chem. Commun.* **2024**, *60* (11), 1468–1471. <https://doi.org/10.1039/D3CC05000A>.
- (18) Sugiura, K. [2.2]Paracyclophane-Based Chiral Platforms for Circularly Polarized Luminescence Fluorophores and Their Chiroptical Properties: Past and Future. *Front. Chem.* **2020**, *8*. <https://doi.org/10.3389/fchem.2020.00700>.
- (19) Gon, M.; Morisaki, Y.; Chujo, Y. Optically Active Cyclic Compounds Based on Planar Chiral [2.2]Paracyclophane: Extension of the Conjugated Systems and Chiroptical Properties. *J. Mater. Chem. C* **2014**, *3* (3), 521–529. <https://doi.org/10.1039/C4TC02339K>.
- (20) Weiland, K. J.; Gallego, A.; Mayor, M. Beyond Simple Substitution Patterns – Symmetrically Tetrasubstituted [2.2]Paracyclophanes as 3D Functional Materials. *Eur. J. Org. Chem.* **2019**, *2019* (20), 3073–3085. <https://doi.org/10.1002/ejoc.201900061>.
- (21) Rapp, M. R.; Leis, W.; Zinna, F.; Di Bari, L.; Arnold, T.; Speiser, B.; Seitz, M.; Bettinger, H. F. Bright Luminescence by Combining Chiral [2.2]Paracyclophane with a Boron–Nitrogen-Doped Polyaromatic Hydrocarbon Building Block. *Chem. – Eur. J.* **2022**, *28* (11), e202104161. <https://doi.org/10.1002/chem.202104161>.
- (22) Ishioka, S.; Hasegawa, M.; Hara, N.; Sasaki, H.; Nojima, Y.; Imai, Y.; Mazaki, Y. Chiroptical Properties of Oligophenylenes Anchoring with Stereogenic [2.2]Paracyclophane. *Chem. Lett.* **2019**, *48* (7), 640–643. <https://doi.org/10.1246/cl.190149>.
- (23) Xu, W.; Yang, X.-D.; Fan, X.-B.; Wang, X.; Tung, C.-H.; Wu, L.-Z.; Cong, H. Synthesis and Characterization of a Pentiptycene-Derived Dual Oligoparaphenylene Nanohoop. *Angew. Chem. Int. Ed.* **2019**, *58* (12), 3943–3947. <https://doi.org/10.1002/anie.201814482>.
- (24) Krzeszewski, M.; Ito, H.; Itami, K. Infinitene: A Helically Twisted Figure-Eight [12]Circulene Topoisomer. *J. Am. Chem. Soc.* **2022**, *144* (2), 862–871. <https://doi.org/10.1021/jacs.1c10807>.
- (25) Stępień, M.; Sprutta, N.; Latos-Grażyński, L. Figure Eights, Möbius Bands, and More: Conformation and Aromaticity of Porphyrinoids. *Angew. Chem. Int. Ed.* **2011**, *50* (19), 4288–4340. <https://doi.org/10.1002/anie.201003353>.
- (26) Nie, H.; Li, Q.-H.; Zhang, S.; Wang, C.-M.; Lin, W.-H.; Deng, K.; Shu, L.-J.; Zeng, Q.-D.; Wan, J.-H. Figure-Eight Arylene Ethynylene Macrocycles: Facile Synthesis and Specific Binding Behavior toward Hg^{2+} . *Org. Chem. Front.* **2021**, *8* (24), 6806–6815. <https://doi.org/10.1039/D1QO00812A>.
- (27) Schaub, T. A.; Prantl, E. A.; Kohn, J.; Bursch, M.; Marshall, C. R.; Leonhardt, E. J.; Lovell, T. C.; Zakharov, L. N.; Brozek, C. K.; Waldvogel, S. R.; Grimme, S.; Jasti, R. Exploration of the Solid-State Sorption Properties of Shape-Persistent Macrocyclic Nanocarbons as Bulk Materials and Small Aggregates. *J. Am. Chem. Soc.* **2020**, *142* (19), 8763–8775. <https://doi.org/10.1021/jacs.0c01117>.
- (28) Palomo, L.; Favereau, L.; Senthilkumar, K.; Stępień, M.; Casado, J.; Ramírez, F. J. Simultaneous Detection of Circularly Polarized Luminescence and Raman Optical Activity in an Organic Molecular Lemniscate. *Angew. Chem. Int. Ed.* **2022**, *61* (34), e202206976. <https://doi.org/10.1002/anie.202206976>.
- (29) Wang, L.-H.; Hayase, N.; Sugiyama, H.; Nogami, J.; Uekusa, H.; Tanaka, K. Synthesis, Structures, and Properties of Highly Strained Cyclophenylene–Ethynylenes with Axial and Helical Chirality. *Angew. Chem. Int. Ed.* **2020**, *59* (41), 17951–17957. <https://doi.org/10.1002/anie.202006959>.
- (30) Senthilkumar, K.; Kondratowicz, M.; Lis, T.; Chmielewski, P. J.; Cybińska, J.; Zafra, J. L.; Casado, J.; Vives, T.; Crassous, J.; Favereau, L.; Stępień, M. Lemniscular [16]Cycloparaphenylene: A Radially Conjugated Figure-Eight Aromatic Molecule. *J. Am. Chem. Soc.* **2019**, *141* (18), 7421–7427. <https://doi.org/10.1021/jacs.9b01797>.
- (31) Wu, Y.; Zhuang, G.; Cui, S.; Zhou, Y.; Wang, J.; Huang, Q.; Du, P. Through-Space π -Delocalization in a Conjugated Macrocyclic Consisting of [2.2]Paracyclophane. *Chem. Commun.* **2019**, *55* (97), 14617–14620. <https://doi.org/10.1039/C9CC06492C>.
- (32) Fan, Y.; He, J.; Liu, L.; Liu, G.; Guo, S.; Lian, Z.; Li, X.; Guo, W.; Chen, X.; Wang, Y.; Jiang, H. Chiral Carbon Nanorings: Synthesis, Properties and Hierarchical Self-Assembly of Chiral Ternary Complexes Featuring a Narcissistic Chiral Self-Recognition for Chiral Amines. *Angew. Chem. Int. Ed.* **2023**, *62* (28), e202304623. <https://doi.org/10.1002/anie.202304623>.

- (33) Weiland, K. J.; Brandl, T.; Atz, K.; Prescimone, A.; Häussinger, D.; Šolomek, T.; Mayor, M. Mechanical Stabilization of Helical Chirality in a Macrocyclic Oligothiophene. *J. Am. Chem. Soc.* **2019**, *141* (5), 2104–2110. <https://doi.org/10.1021/jacs.8b11797>.
- (34) Sisto, T. J.; Golder, M. R.; Hirst, E. S.; Jasti, R. Selective Synthesis of Strained [7]Cycloparaphenylene: An Orange-Emitting Fluorophore. *J. Am. Chem. Soc.* **2011**, *133* (40), 15800–15802. <https://doi.org/10.1021/ja205606p>.
- (35) Kręćjasz, R. B.; Malinčík, J.; Šolomek, T. Exploring Silyl Protecting Groups for the Synthesis of Carbon Nanohoops. *Synthesis* **2023**, *55* (9), 1355–1366. <https://doi.org/10.1055/a-2008-9505>.
- (36) He, J.; Yu, M.; Pang, M.; Fan, Y.; Lian, Z.; Wang, Y.; Wang, W.; Liu, Y.; Jiang, H. Nanosized Carbon Macrocycles Based on a Planar Chiral Pseudo Meta-[2.2]Paracyclophane. *Chem. – Eur. J.* **2022**, *28* (13), e202103832. <https://doi.org/10.1002/chem.202103832>.
- (37) Kubo, H.; Shimizu, D.; Hirose, T.; Matsuda, K. Circularly Polarized Luminescence Designed from Molecular Orbitals: A Figure-Eight-Shaped [5]Helicene Dimer with D₂ Symmetry. *Org. Lett.* **2020**, *22* (23), 9276–9281. <https://doi.org/10.1021/acs.orglett.0c03506>.
- (38) König, B.; Knieriem, B.; Meijere, A. D. Double-Layered 1,4-Distyrylbenzene Chromophores–Synthesis, UV and Fluorescence Spectra. *Chem. Ber.* **1993**, *126* (7), 1643–1650. <https://doi.org/10.1002/cber.19931260723>.
- (39) Krasnova, I. Yu.; Antonov, D. Yu.; Shapovalov, A. V.; Shifrina, Z. B. Dendritic Polyphenylene Framework as a Light-Harvesting Shell for Highly Emissive [2.2]Paracyclophane Core. *Polymer* **2021**, *234*, 124227. <https://doi.org/10.1016/j.polymer.2021.124227>.
- (40) Jasti, R.; Bhattacharjee, J.; Neaton, J. B.; Bertozzi, C. R. Synthesis, Characterization, and Theory of [9]-, [12]-, and [18]Cycloparaphenylene: Carbon Nanohoop Structures. *J. Am. Chem. Soc.* **2008**, *130* (52), 17646–17647. <https://doi.org/10.1021/ja807126u>.
- (41) Sibbel, F.; Matsui, K.; Segawa, Y.; Studer, A.; Itami, K. Selective Synthesis of [7]- and [8]Cycloparaphenylenes. *Chem. Commun.* **2013**, *50* (8), 954–956.
- (42) Xia, J.; Jasti, R. Synthesis, Characterization, and Crystal Structure of [6]Cycloparaphenylene. *Angew. Chem.* **2012**, *124* (10), 2524–2526. <https://doi.org/10.1002/ange.201108167>.
- (43) Patel, V. K.; Kayahara, E.; Yamago, S. Practical Synthesis of [n]Cycloparaphenylenes (N=5, 7–12) by H₂SnCl₄-Mediated Aromatization of 1,4-Dihydroxycyclo-2,5-Diene Precursors. *Chem. – Eur. J.* **2015**, *21* (15), 5742–5749. <https://doi.org/10.1002/chem.201406650>.
- (44) He, J.; Yu, M.-H.; Lian, Z.; Fan, Y.-Q.; Guo, S.-Z.; Li, X.-N.; Wang, Y.; Wang, W.-G.; Cheng, Z.-Y.; Jiang, H. Lemniscular Carbon Nanohoops with Contiguous Conjugation from Planar Chiral [2.2]Paracyclophane: Influence of the Regioselective Synthesis on Topological Chirality. *Chem. Sci.* **2023**, *14* (16), 4426–4433. <https://doi.org/10.1039/D2SC06825G>.
- (45) Lovell, T. C.; Fosnacht, K. G.; Colwell, C. E.; Jasti, R. Effect of Curvature and Placement of Donor and Acceptor Units in Cycloparaphenylenes: A Computational Study. *Chem. Sci.* **2020**, *11* (44), 12029–12035. <https://doi.org/10.1039/D0SC03923C>.
- (46) Stawski, W.; Van Raden, J. M.; Patrick, C. W.; Horton, P. N.; Coles, S. J.; Anderson, H. L. Strained Porphyrin Tape–Cycloparaphenylene Hybrid Nanorings. *Org. Lett.* **2023**, *25* (2), 378–383. <https://doi.org/10.1021/acs.orglett.2c04089>.
- (47) Popova, E.; Antonov, D.; Sergeeva, E.; Vorontsov, E.; Stash, A.; Rozenberg, V.; Hopf, H. New Monomers for Organometallic Poly-p-Xylylenes: Synthesis of Silyl-, Germyl- and Stannyl[2.2]Paracyclophane Derivatives. *Eur. J. Inorg. Chem.* **1998**, *1998* (11), 1733–1737. [https://doi.org/10.1002/\(SICI\)1099-0682\(199811\)1998:11%253C1733::AID-EJIC1733%253E3.0.CO;2-H](https://doi.org/10.1002/(SICI)1099-0682(199811)1998:11%253C1733::AID-EJIC1733%253E3.0.CO;2-H).

